2009-06-22

Applications of Variation Analysis Methods to Automotive Mechanisms

Robert C. Leishman
Brigham Young University - Provo

APPLICATIONS OF VARIATION ANALYSIS METHODS TO AUTOMOTIVE MECHANISMS

by

Robert C. Leishman

A thesis submitted to the faculty of

Brigham Young University

in partial fulfillment of the requirements for the degree of

Master of Science

Department of Mechanical Engineering

Brigham Young University

August 2009

BRIGHAM YOUNG UNIVERSITY

GRADUATE COMMITTEE APPROVAL

of a thesis submitted by

Robert C. Leishman

This thesis has been read by each member of the following graduate committee and by majority vote has been found to be satisfactory.

Date	Kenneth W. Chase, Chair
Date	C. Gregory Jensen
Date	Mark Colton

BRIGHAM YOUNG UNIVERSITY

As chair of the candidate's graduate committee, I have read the thesis of Robert C. Leishman in its final form and have found that (1) its format, citations, and bibliographical style are consistent and acceptable and fulfill university and department style requirements; (2) its illustrative materials including figures, tables, and charts are in place; and (3) the final manuscript is satisfactory to the graduate committee and is ready for submission to the university library.

Date

Kenneth W. Chase
Chair, Graduate Committee

Accepted for the Department

Tim W. McLain
Department Chair

Accepted for the College

Alan R. Parkinson
Dean, Ira A. Fulton College of
Engineering and Technology

ABSTRACT

APPLICATIONS OF VARIATION ANALYSIS METHODS TO AUTOMOTIVE MECHANISMS

Robert C. Leishman

Department of Mechanical Engineering

Master of Science

Variation analysis, or tolerance analysis as it is sometimes called, is typically used to predict variation in critical dimensions in assemblies by calculating the stack-up of the contributing component variations. It is routinely used in manufacturing and assembly environments with great success. Design engineers are able to account for the small changes in dimensions that naturally occur in manufacturing processes, in equipment, and due to operators and still ensure that the assemblies will meet the design specifications and required assembly performance parameters. Furthermore, geometric variation not only affects critical fits and clearances in static assemblies, it can also cause variation in the motion of mechanisms, and their dynamic performance. The fact that variation and motion analysis are both dependent upon the geometry of the assembly makes this area of study much more challenging.

This research began while investigating a particular application of dynamic assemblies - automobiles. Suspension and steering systems are prime examples dynamic assemblies. They are also critical systems, for which small changes in dimension can cause dramatic changes in the vehicle performance and capabilities. The goals of this research

were to develop the tools necessary to apply the principles of static variation analysis to the kinematic motions of mechanisms. Through these tools, suspension and steering systems could be analyzed over a range of positions to determine how small changes in dimensions could affect the performance of those systems.

There are two distinct applications for this research, steering systems and suspension systems. They are treated separately, as they have distinct requirements. Steering systems are mechanisms, for which position information is most critical to performance. In suspension systems, however, the higher order kinematic terms of velocity and acceleration often are more important than position parameters.

ACKNOWLEDGMENTS

First of all, I would like to thank my wife, Lisa, for all the support that she gives me, without it I would never have gotten this far. I love her “with all my heart”.

Secondly, I would like to thank Dr. Ken Chase for his patience and guidance - and tireless editing of my writing. What an excellent advisor and mentor he has been to me. I really appreciated the weekly meetings we had, to keep me on task!

And most importantly, I would like to thank my Heavenly Father for providing me the opportunities and blessings that I have received. Without His help, I never would have figured any of this out.

Table of Contents

List of Tables

List of Figures

Chapter 1

Introduction

Variation analysis, or tolerance analysis as it is sometimes called, is typically used to predict variation in critical dimensions in assemblies by calculating the stack-up of the contributing component variations. It is routinely used in manufacturing and assembly environments with great success. Design engineers are able to account for the small changes in dimensions that naturally occur in manufacturing processes, in equipment, and due to operators and still ensure that the assemblies will meet the design specifications and required assembly performance parameters. Furthermore, geometric variation not only affects critical fits and clearances in static assemblies, it can also cause variation in the motion of mechanisms, and their dynamic performance. The fact that variation and motion analysis are both dependent upon the geometry of the assembly makes this area of study much more challenging.

This research began while investigating a particular application of dynamic assemblies - automobiles. Suspension and steering systems are prime examples dynamic assemblies. They are also critical systems, for which small changes in dimension can cause dramatic changes in the vehicle performance and capabilities. The goals of this research were to develop the tools necessary to apply the principles of static variation analysis to the kinematic motions of mechanisms. Through these tools, suspension and steering systems could be analyzed over a range of positions to determine how small changes in dimensions could affect the performance of those systems.

There are two distinct applications for this research, steering systems and suspension systems. They are treated separately, as they have distinct requirements. Steering systems are mechanisms, for which position information is most critical to performance.

In suspension systems, however, the higher order kinematic terms of velocity and acceleration often are more important than position parameters.

1.1 Scope

Steering and suspension systems are very broad topics and incorporate many different areas of potential analysis. As the research proceeded, it became clear that only parts of the whole would be achievable for the scope of this work.

Because of needs observed with the BYU Formula One Racing Team, the steering approach became one of a design tool. The objective was to develop a tool that could synthesize a steering mechanism, analyze its performance, and provide variational analysis capabilities. Team members would be able to quantify how variations due to manufacturing capabilities would affect the performance of the system.

Suspension systems are dynamic. Acceleration information is very important, as it relates to the forces observed on the tires and structural members. The focus for this topic of the research was to develop a comprehensive model for the effects dimensional variations have on the position, velocity, and acceleration of critical components.

1.2 Literature Review

Previous work by other researchers has been completed in the focus areas of this research and has contributed to this work. This section documents previous studies and provides the setting for this work.

1.2.1 Steering Literature Review

Several researchers have approached the design problem of synthesizing a mechanism for rack and pinion steering systems.

Zarak and Townsend [1] used optimization methods to synthesize side take off (STO) leading or trailing configuration steering systems. The approach is valid and provides for optimal designs. However, they use an impractical error function composed of

the differences in the turning radii. Thus, results do not relate back to practical information available to designers, like rack travel and steering angle.

Simonescu and Smith [2] also used optimization methods to synthesize the linkages, using three geometric parameters. Both central take off (CTO) and STO linkages are synthesized; however, only leading configurations are considered. They used the "method of increasing the degrees of freedom" combined with cognates to find optimum values for the linkages. The output of the research is a series of design charts for different scenarios. The charts provide valuable design information. However, if a desired design space is outside those portrayed in the example, the designer would have to contact the authors or recreate the computer routines.

Simonescu and Beale [3] use optimization synthesis of a four bar linkage to provide the mechanism for Ackermann steering. The article discusses many different objective functions that can be used to converge to an optimum linkage. A sensitivity analysis discussion is also presented, but concludes that small changes do not practically change the steering error. The end product for the design engineer is also a series of 3D design charts for leading and trailing linkage designs. These charts are difficult to read, and inaccurate readings may produce sub-optimal linkage designs.

Hanzaki and Saha [4] use a similar method as [2] to complete a preliminary optimization of CTO and STO, forward and trailing steering linkages; only, three lengths are used as parameters. Afterward, a sensitivity analysis of the steering linkages to tolerances, assembly errors, and clearances is performed. Then, the linkages are re-optimized for minimal steering error and sensitivity. The only mark against the research is that no design charts or tools, besides the published equations, are offered to the design engineer.

All of the above research has been accomplished with the primary goals being the synthesis and the optimization methods. None of the previous research is geared toward providing accessible, easy-to-use information for the design engineer.

1.2.2 Suspension Literature Review

The tolerance analysis method, known as the Direct Linearization Method (DLM), that this work builds upon was originally introduced in [5]. Chase *et al.*, further developed

the method, which uses vector-loop assembly models and loop equations [6], much like those used in kinematics [7]. The work provides a closed-form method for determining the variation in the critical parameters of a static assembly due to the length and angular variations of the contributing parts. The method requires only two computations - one for the mean and one for the variations. This method was also extended, without too much modification, to three-dimensional assemblies [8].

Later, Chase *et al.*, presented a method for including the ANSI 14.5 geometric feature variations in the DLM [9]. They found that the geometric feature variations can accumulate statistically and propagate kinematically in assemblies just like dimensional variations. They claimed that geometric variations are independent of those produced by length and angular variation, when geometric features are applied to surfaces of mating parts. They showed that geometric feature variations may be characterized by how they transmit variation between parts, or in other words, through the joints.

Brown [10] modeled clearance effects in pin joints as two orthogonal geometric feature variations, inserted at the joint centers. In this way, the clearances remained independent of the length variations. The product of sensitivity times tolerance could be added linearly for worst case or using root-sum-squares for statistical variation analysis, just like what is done for normal length and angular variations.

Faerber [11], did work that illustrated the mathematical similarity between velocity and position variation. He showed that the 2D DLM could be performed by kinematic solvers like ADAMS. This was accomplished using what Faerber called *equivalent mechanisms*. By adding fictitious joints to a static assembly, he created a mechanism whose velocity Jacobian was identical to the tolerance sensitivity matrix. What appeared to be mechanisms to the solver, in reality expressed the changes in length and angle in a static assembly due to variations. Dabling [12] extended this work to 3D and added equivalent mechanisms for each of the geometric feature variations. The methods that they developed are only applicable to positional variation.

Wittwer *et al.*, applied the DLM to mechanism position analysis [13]. They also analyzed the differences between the bivariate DLM and deterministic and other probabilistic methods. However, the ability to account for joint variation through the use of geometric

feature variations or other methods was not included. Other researchers have approached this problem in a similar manner [14, 15].

Many other researchers have taken the next step and added the capability to model joint clearances to mechanism position variation analysis [16–19]. This type of analysis is very common in the robotics field. These analysis are all only applicable to position variation and do not examine the effects of geometric variations on higher order kinematic terms.

Lee and Gilmore [20] have developed a comprehensive, closed form method that finds position, velocity, and acceleration variations of open and closed loop mechanisms. However, an effective link length model is used to account for variations due to pin joint clearances, which combines the clearance with an associated link length. This made the clearances dependent on the link length variations. No other joint variations can be accounted for in this method. They were able to extend their method to dynamic analysis, including forces and moments in the tolerance analysis, [21].

1.3 Research Objectives

The following are the objectives for the research documented in this Thesis.

1.3.1 Objectives - Steering

The objectives of the steering system research is to create an easy-to-use design and analysis tool with the following capabilities:

1. Use the tool to synthesize either leading or trailing, CTO or STO steering system configurations.

2. Provide optimization to quickly and efficiently converge to the best possible solution given multiple constraints.

3. Ability to see the effects of tolerances and pin clearances on the design.

4. Ability to adjust the percentage of Ackermann steering.

5. Visually display the structural error of the system and how tolerances affect that error throughout the range of the steering angle.

1.3.2 Objectives - Suspension

The objectives for the suspension portion of the research are to:

1. Build on the DLM by providing the capability to analyze the variations in position, velocity, and acceleration of any open or closed loop 2D mechanism.

2. Add the capability to describe the effects of geometric feature variations on the variations of position, velocity, and acceleration of any open or closed loop 2D mechanism.

1.4 Thesis Overview

The remaining chapters in this thesis are organized as follows. Chapter 2 discusses the background and new theory developed for the steering design tool. It contains an example of how steering system synthesis is accomplished using this new method. Chapter 3 discusses all the features of the steering design tool using an extended example. Chapter 4 goes through the background of the DLM and the derivation to apply the DLM to mechanism position, velocity, and acceleration analysis. An example is worked to show how the DLM can be used to quantitatively understand the effects of geometric variations on mechanism kinematics. Chapter 5 derives the procedure for applying geometric feature variations to characterize the variations from different 2D kinematic joints. An example that illustrates that joint variations do impact position, velocity, and acceleration variation is included. Finally, Chapter 6 contains the concluding remarks and the recommendations for future research.

Chapter 2

Rack and Pinion Steering Linkage Synthesis Using an Adapted Freudenstein Approach

2.1 Introduction

Automobile steering systems have a straightforward purpose: angle the tires so that the vehicle can proceed in the desired direction safely and under full control. To accomplish this function, many different steering designs have been devised. Each accomplishes the basic purpose in a slightly distinct manner [22,23]. Arguably the most widely implemented are rack and pinion steering systems. A steering system must be modeled and designed for each vehicle. Even though they have the same basic components, each vehicle requires a slightly different system. Vehicle models all have slightly different lengths and widths, and more importantly, different suspension systems and physical space constraints, which make it necessary for each steering system to be somewhat unique. Even small changes in dimensions can dramatically alter steering performance. Thus, it is essential to have available a simple, easy-to-use design tool that enables designers to quickly iterate and converge to optimal steering solutions by changing only those few parameters or constraint values that drive the iteration. This Chapter is based on an article previously published by the author, [24].

Typical rack and pinion systems, shown in Figs. 2.1 and 2.2, consist of a straight gear (rack), which is driven by the steering gear (pinion), back and forth. Tie rods connect the rack to the steering arms, which connect to the wheel uprights and cause the wheels to turn. The axis of rotation of the upright is known as the *kingpin axis*. There are two main types of rack and pinion linkages: Fig. 2.1: central take-off (CTO), where the tie rods connect at the center point of the rack and Fig. 2.2: side take-off (STO), where the tie rods

connect to the ends of the rack. They can both be placed in either a trailing or leading configuration, Fig. 2.3.

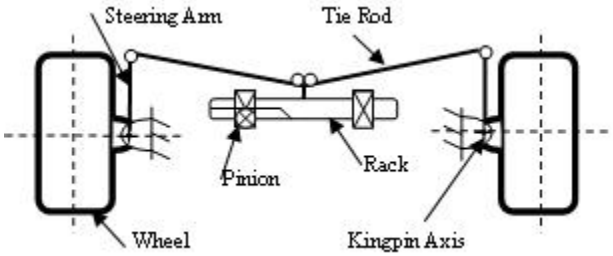

Figure 2.1: Central take off rack and pinion steering top view

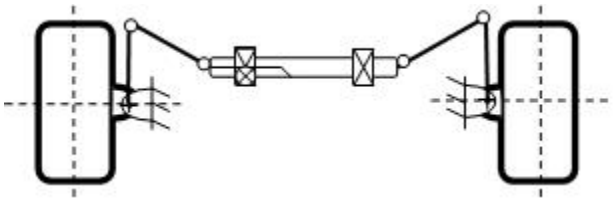

Figure 2.2: Side take off rack and pinion steering top view

2.1.1 Assumptions

Sometimes the kingpin axis is inclined by both the caster and kingpin inclination angles, making the steering system a three dimensional mechanism. This paper discusses the design and analysis of planar steering mechanisms; consequently, three dimensional steering systems are outside the scope of this work.

The tie rods and steering arms are considered rigid for the work presented here. In actual performance, these members might flex and bend, altering the calculated performance.

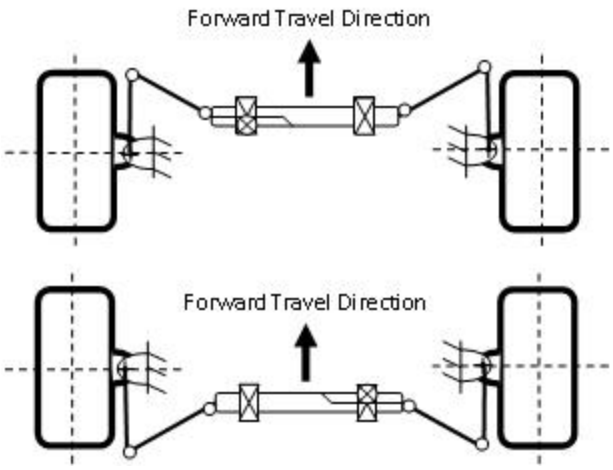

Figure 2.3: Leading (top) and trailing (bottom) steering systems

2.1.2 Ackermann Steering

An important aspect of steering systems is the Ackermann principle [25–27], illustrated in Fig. 2.4 . In essence, it provides the necessary steering angles for the tires to provide pure rolling during a turn and not scrub. Today, it is sometimes used more as a metric and a factor for comparison than a critical parameter, but it is still in use. This is especially true in motor vehicle racing, where different levels, or even negative Ackermann steering, is sometimes desired [28]. Equation 2.1 gives the formula for obtaining Ackermann geometry during a turn, where θ_o is the outside wheel angle, θ_i is the inside wheel angle, W_k is the kingpin width, and W_b is the wheelbase, as shown in Fig 2.4.

In this study, the formula for Ackermann steering has been simplified by using the kingpin width, W_k, instead of the width of the contact patches, or track-width, W_t. This approximation allows the vehicle width and length to remain constant over a full turn. In order to make sure that the kingpin width simplification could be applied, a sensitivity analysis of the inside and outside turn angles with respect to small changes to the width and height of the vehicle was completed. It was found that for a large turn radius ($\geq$ 100 ft), the changes were negligible, 0.04 degrees per inch of offset (deg/in) or less. For a turn radius at and below 20 ft, the sensitivities increased to more significant levels, about 0.15 to 0.30 deg/in. This simplification is valid for the most common applications - only

during slow, very tight corners of small vehicles does the simplification break down. This simplification has also been used by other researchers [2–4, 25, 26].

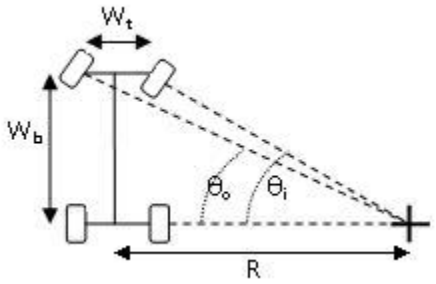

Figure 2.4: Top view of Ackermann steering geometry

$$\begin{aligned} tan(\theta_o) &= \frac{W_b}{R+\frac{W_k}{2}} \\ tan(\theta_i) &= \frac{W_b}{R-\frac{W_k}{2}} \\ \theta_i &= atan\left(\frac{W_b}{\frac{W_b}{tan(\theta_o)}-W_k}\right) \end{aligned} \tag{2.1}$$

As can be seen in Fig. 2.4, the basic requirement is that all four tire axes intersect at a common point. The vehicle is then in pure rotation about that point. It should also be noted that the front tires are not parallel during a turn of any radius. Even when steering straight ahead, the front tire axes often are not exactly parallel due to *static toe*, which makes the steering more stable, [25]. Static toe is where the tires are turned in or out slightly.

2.1.3 Research

This research proposes using a simple and novel way to model and optimize a rack and pinion steering system. Two crank and slider mechanisms are combined to make a double crank and single slider mechanism. The input for the mechanism is the slider (the

rack and pinion) and the outputs are the two crank angles, which correspond to the steering angles. To assist in the optimization of the linkages, Freudenstein's equation [29, 30] for the synthesis of a mechanism has been adapted for a crank and slider mechanism. By using the Freudenstein equation to help constrain the synthesis, optimization can be very quickly and easily applied to find an ideal solution; even when the system is restricted by physical constraints. The method is simple enough to be easily implemented on a spreadsheet.

2.2 Freudenstein's Equation

Freudenstein developed a method to synthesize a four-bar mechanism, Fig. 2.5, using a concept called precision points, [29, 30]. The horizontal (X) and vertical (Y) position loop equations, Eqns. 2.2 and 2.3 are combined to eliminate one of the angle parameters (θ) and simplify the synthesis.

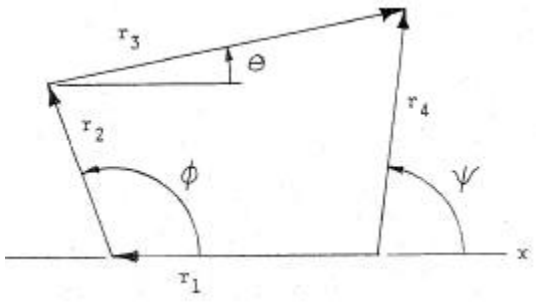

Figure 2.5: Four-bar mechanism

$$X \quad \Rightarrow \quad r_1 - r_2 cos(\phi) - r_3 cos(\theta) = r_4 cos(\psi) = 0 \tag{2.2}$$

$$Y \quad \Rightarrow \quad r_2 sin(\phi) + r_3 sin(\theta) = r_4 sin(\psi) = 0 \tag{2.3}$$

The result is called Freudenstein's equation, Eqn. 2.4.

$$R_1 cos(\psi) - R_2 cos(\phi) + R_3 = cos(\phi - \psi) \tag{2.4}$$

The link length terms are grouped together to form the three unknown constants, R_1, R_2, and R_3, Eqns. 2.5 - 2.7.

$$R_1 = \frac{r_1}{r_2} \tag{2.5}$$

$$R_2 = \frac{r_1}{r_4} \tag{2.6}$$

$$R_3 = \frac{r_1^2 + r_2^2 + r_4^2 - r_3^2}{2r_2r_4} \tag{2.7}$$

The three unknown constants are resolved by setting up three position equations at three selected precision points. This is usually set up by establishing base values for the crank angles, ϕ_0 and ψ_0, and increment values, $\Delta\phi$ and $\Delta\psi$. The base value is incremented one time to obtain the second precision point and then incremented again to obtain the third precision point. These points are on the function that the designer wants the mechanism to follow. At the three points, the error, or the difference between the actual position of the mechanism and the desired position, is zero. The resulting system of equations is solved simultaneously for the R values. The link lengths are then back solved from the three R values. Length r_1 can then be used to scale the mechanism.

Choosing Chebychev [30] spacing for the precision points, Eqn. 2.8, helps to reduce the overall error by equalizing the spacing between the points.

$$X_i = \frac{X_{MAX} + X_0}{2} - \frac{X_{MAX} - X_0}{2} cos\left(\frac{(2j-1)\pi}{2n}\right), (j = 1,2,3) \tag{2.8}$$

X_i is the i^{th} variable (in this case either ϕ or ψ), X_{MAX} is the maximum value possible for that precision point, X_0 is the minimum value, j is the j^{th} precision point, and n is three (for three precision points).

Although this solution does not always give an optimum location for the precision points, it does give a good starting point. By systematically iterating the positions of the precision points, the error can be minimized across the desired range of the mechanism. The optimum spacing is reached when the max error between the precision points and the two ends of the range are all equal. This, however, is only the optimum for the selected input and output crank angles, as defined by the starting angles ϕ_0 and ψ_0 and ranges

$\Delta\phi$ and $\Delta\psi$. Other design factors must be considered in selecting these factors, such as the specified extremes of turning radius, acceptable lengths for the two cranks, and maintaining a transmission angle centered near 90^o.

2.2.1 Freudenstein's Equations Applied to Slider-Crank Mechanisms

A special case of Freudenstein's equation may be applied to a slider-crank mechanism, Fig. 2.6. For the steering linkage, the input is the ground link L_g, rather than an angle. The output is the crank angle ϕ. The 2-D position loop equation of the mechanism is resolved into two scalar equations - the sum of the X components and the sum of the Y components, Eqns. 2.9 and 2.10.

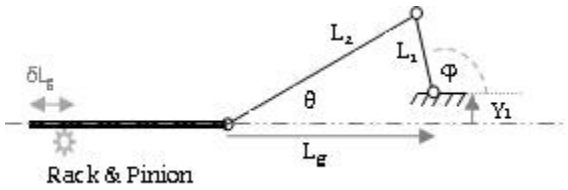

Figure 2.6: A slider-crank mechanism

$$X \quad \Rightarrow \quad L_2 cos(\theta) - L_1 cos(\phi) - L_g = 0 \tag{2.9}$$

$$Y \quad \Rightarrow \quad L_2 sin(\theta) - L_1 sin(\phi) - Y1 = 0 \tag{2.10}$$

Both equations are solved for the L_2 terms, squared and added, resulting in Eqn. 2.11. This step eliminates θ from the equation.

$$L_2^2 = L_1^2 + L_g^2 + Y_1^2 + 2L_1 L_g cos(\phi) + 2L_1 Y_1 sin(\phi) \tag{2.11}$$

Next, the constant terms are grouped into three values: R_1, R_2, and R_3, resulting in the slider-crank form of Freudenstein's equation, Eqn. 2.12.

$$-sin(\phi) = R_1 L_g cos(\phi) + R_2 L_g^2 + R_3 \tag{2.12}$$

$$R_1 = \frac{1}{Y_1} \tag{2.13}$$

$$R_2 = \frac{1}{2L_1Y_1} \tag{2.14}$$

$$R_3 = \frac{L_1^2+Y_1^2-L_2^2}{2L_1Y_1} \tag{2.15}$$

Because there are three unknowns, there must be three equations. The same equation is repeated three times - for three selected precision points for ϕ and L_g.

$$\begin{aligned} -sin(\phi_1) &= R_1L_{g1}cos(\phi_1)+R_2L_{g1}^2+R_3 \\ -sin(\phi_2) &= R_1L_{g2}cos(\phi_2)+R_2L_{g2}^2+R_3 \\ -sin(\phi_3) &= R_1L_{g3}cos(\phi_3)+R_2L_{g3}^2+R_3 \end{aligned} \tag{2.16}$$

The three unknowns, R_1, R_2, and R_3, are found by matrix algebra. The R value's are then converted back to the constant lengths of the mechanism, L_1, L_2, Y_1, using Eqns. 2.17 - 2.19.

By changing the precision points, new mechanisms are synthesized. Not all solutions are valid. Each linkage must be checked to assure no *dead points* (where the angle between L_1 and L_2 goes through zero or 180^o) are encountered over the full range of ϕ. Furthermore, for smooth operation, the preferred angle between L_1 and L_2 (transmission angle) should be kept near 90^o throughout the specified turning angle range.

$$Y_1 = \frac{1}{R_1} \tag{2.17}$$

$$L_1 = \frac{R_1}{2R_2} \tag{2.18}$$

$$L_2 = \sqrt{\frac{1}{R_1^2}+\frac{R_1^2}{4R_2^2}-\frac{R_3}{R_2}} \tag{2.19}$$

2.3 Optimization

Every linkage synthesized by Freudenstein's equation will satisfy the Ackermann requirement at the three selected precision points. At all other crank positions there will be

an error in the steering angle ϕ corresponding to intermediate L_g inputs. The challenge is to find an acceptable linkage which minimizes the steering error over the full range.

The procedure to find an optimum steering system is completed by using the Ackermann equation and loop equations to solve for the error in the steering angle at intermediate points. A square root sum of the squared error over the mechanisms range is the objective function to minimize, Eqn. 2.20.

$$Sum = \sum_{i=1}^{n} \sqrt{(\phi desired_i - \phi actual_i)^2} \tag{2.20}$$

The only parameters that must be varied are the precision points of ϕ and L_g. As mentioned above, the points provided by the Chebychev equation provide excellent starting points for the optimization. Constraints can easily be implemented on the outputs if there are physical limitations on the lengths of the tie rods, steering arms, or off-sets.

However, by combining the two mechanisms together, thereby syncing the left and right wheels, several non-intuitive constraints are developed in the mechanism. The mechanisms are combined by the Ackermann steering objective function, and the inside wheel is dependent on the outside wheel angle.

There are two interesting results from these constraints. First, it was discovered that the middle precision point must correspond to the desired center point of the steering system (the angle for straight travel). If it is set to a random point, the steering error will not be zero for straight ahead driving, and this is not desirable. There are two cases where the center point would not be 90^o: when a certain amount of static toe is desired, and when the steering arm is not parallel to the tire, but is offset by an angle ϕ_0. This can easily be incorporated by just holding the center precision point constant at the desired static toe value or at the offset angle ϕ_0, Fig. 2.7. With the center precision point held constant, only four values need to be varied to find an optimum linkage, ϕ_1, ϕ_3, L_{g1}, and L_{g3}. ϕ_0 may also be varied in the optimization as well, if it is not a set parameter.

The next interesting discovery was that the locations where the error is zero do not correspond to where the precision points are placed. When the halves of the steering are decoupled, this does not occur, and the precision points are the locations of zero error. It is

not quite understood why this is the case, but it happens when the two sides are coupled. When optimizing, the zero values often end up being close to the values for the precision points predicted by the Chebychev equations, even though the precision points are at different values - this will be shown in the example below.

This is a challenging optimization problem, because of the symmetry of the combined mechanism. When the right hand linkage is optimized for a right turn, the left tire will not be at a minimum error, because the link lengths of both mechanisms must be identical. The turning angle of the left tire is dictated by the Ackermann angle, so the positions are not optimized. For left turns, the left tire will have minimum error at the three mirror image points the right turn, but then the right tire will not fully meet the Ackermann requirement. This is also illustrated in the example below.

2.4 Example Problem: Optimum Steering Mechanism

This example finds an optimum steering mechanism for a student Formula One race car, Fig. 2.7, subject to a variety of constraints. Along with the properties and constraints in Tables 2.1 and 2.2, it is desired that the car have Ackermann steering across the whole steering range.

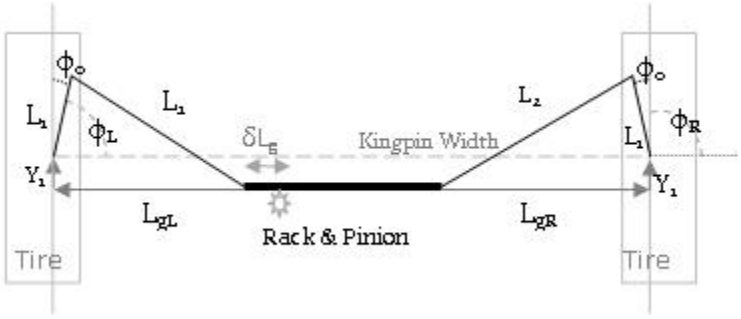

Figure 2.7: Top view of the double slider-crank steering system

The right side parameters (ϕ_R and L_{gR}) are used in the equations to find the optimum linkage. Since the mechanisms are synced, the left side follows the right side. ϕ_0 is positive inward and negative outward.

Table 2.1: Example problem parameters

Vehicle Parameter	Value	Units
Wheelbase	60	in.
Track-width	46.5	in.
Kingpin Width	45	in.
Rack and Pinion Width	13	in.
δL_g	2	in.
ϕ_0	5	deg.
Static Toe	0	deg.
Steering Range (+/-)	20	deg.

Table 2.2: Vehicle constraints

Parameter	Value	Units
Y_1	≤ 7	in.
L_1	≤ 5	in.
L_2	–	in.
ϕ_0	$\geq$ -3	deg.
ϕ_0	≤ 10	deg.

2.4.1 Design Optimization Procedure

A spreadsheet was composed, using Microsoft Excel, to evaluate the example. This spreadsheet is documented in Chapter 3. The modified Freudenstein's equations were set up and solved using the parameters in Table 2.1. The ideal Ackermann angles for the right and left tires were laid out using Eqn. 2.1, as the rack moved right and left through one complete cycle. The outside angle drives the equations (the left wheel on the right turn and the right wheel on the left turn), but the right wheel information is used in the Freudenstein's equations and the solver routine. Alongside this information, the actual steering angles for both wheels were calculated using the loop equations, Eqns 2.9 and 2.10. The sum of structural errors were calculated according to Eqn. 2.20. Initial estimates of the precision points were provided by Chebychev spacing, Eqn. 2.8, and are shown for this example in Table 2.3. This provided a basic mechanism for the steering system.

Excel Solver was used to optimize the linkage for minimum structural error along the whole range of the mechanism. To make sure that a value of "-N/A" would not stop the

solver routine (i.e., the loop equations not being able to close), an *if* statement was used to filter these values to an error of 100. This allowed the solver to continue through all types of linkages without crashing and avoid values where the resulting mechanism could not deliver the desired turn angles. The parameters for the optimized steering system for this configuration are in Table 2.5.

Table 2.3: Chebychev spacing for the precision points, for the preliminary mechanism

Precision Point	ϕ	L_g
1	66.1484^o	14.2679
2	86.5^o	16
3	106.8516^o	17.7321

2.4.2 Example Results

Table 2.4: Final precision point values

Precision Point	ϕ	L_g
1	-1.12499^o	13.41701
2	90^o	16
3	125.3423^o	19.14197

Table 2.5: Results from the optimization

Parameter	**Value**	**Units**
ϕ_0	4.654376	deg
Y_1	6.999998	in
L_1	4.999999	in
L_2	19.66687	in
SSE	4.044683	–

The precision points that the solver moved around to obtain the optimized parameters turned out to be quite different than what the Chebychev spacing values were, Tables 2.4 and 2.3. The values of zero error in Fig. 2.8 are clearly not these values either. However, the Chebychev values are close to the values of zero error. This is what is commonly observed when the two mechanisms are brought together through the objective function.

Figure 2.8 displays the standard right and left wheel angle errors for the optimized mechanism. This is along the change in L_g or ΔL_g, over a full left and right turn. Here it is seen how the error for the left wheel is the mirrored inverse of the right; and how the minimal errors do not occur at the same points for the right and left wheels, except for at the center point.

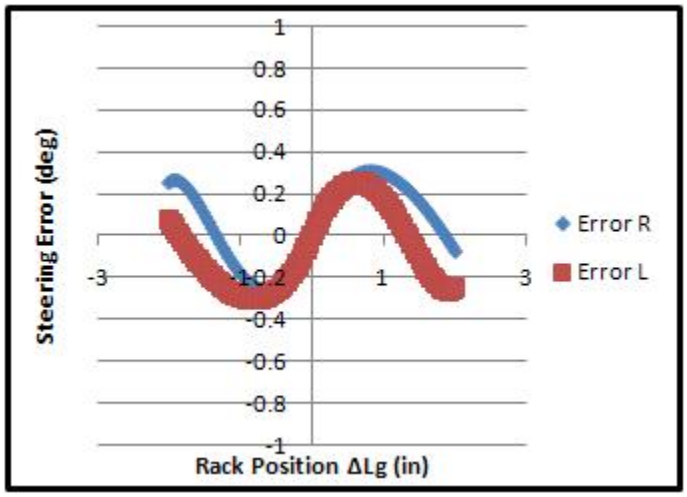

Figure 2.8: Steering angle error for the right and left tires

The steering system error ranges from 0.303 to -0.257 degrees off from an actual Ackermann steering system. These values are within the error that occurs naturally in the steering system due to the difference in the designed dimensions and what the actual built dimensions will be (based on link length tolerances of ± 0.01 in.). For all practical purposes, this car now has 100% Ackermann steering over its entire steering range.

2.4.3 CTO Design and Results

To design a CTO rack and pinion steering system with the same parameters and constraints, the only thing that needs to be modified is the rack width value. This can be shorted to zero if the two joints meet at the same point, or to the value between the two joints. For this example, the value was changed to be one inch. Table 2.6 shows the links for the optimized steering system and Fig. 2.9 shows the error over the steering range, along ΔL_g.

Table 2.6: Results from the optimization for the CTO linkage

Parameter	Value	Units
ϕ_0	3.723086	deg
Y1	6.999998	in
L1	4.999999	in
L2	24.77028	in
SSE	30.06172	–

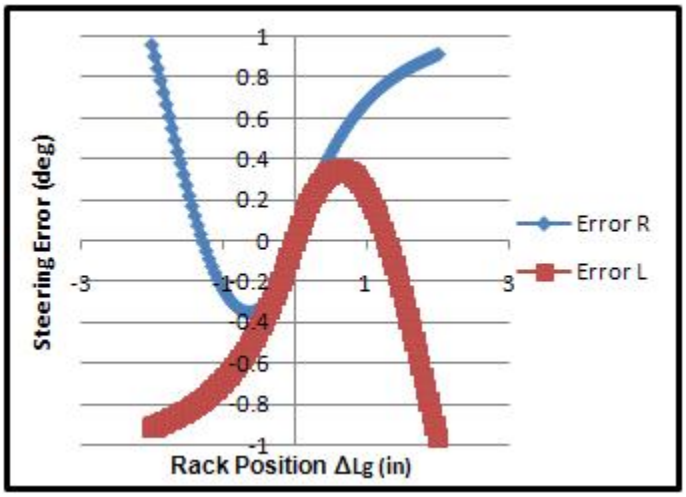

Figure 2.9: Steering angle error for the right and left tires for the CTO linkage design

As is seen in the figure, there are only two points of zero error under these particular constraints. When the constrains are adjusted, some configurations do show three or some-

times even four points of zero error - which brings down the overall error in the steering range. This displays an important point; often times in optimization the constraints limit a design from achieving the optimum value.

2.5 Conclusions

A new method for synthesizing rack and pinion steering systems has been presented in this chapter. It is a combination of classical mechanism synthesis tools and adapted optimization methods. The unique combination allows for quick and easy optimized solutions that can be completed using standard spreadsheet tools. The method is flexible to allow for design of either the CTO or STO rack and pinion steering system in a leading or trailing configuration (The trailing configuration will be shown in the example in Chapter 3). It provides an excellent tool for designers to find optimal preliminary designs and to iterate on those designs as vehicle parameters and spatial constraints evolve.

Chapter 3

Rack and Pinion Steering Mechanism Design and Analysis Tool

3.1 Introduction

As mentioned in Chapter 2, the methodology behind the steering design tool merges classical Freudenstein synthesizing theory with an optimization routine to provide quick results. The method uses preselected *precision points* from Freudenstein's equation to synthesize the mechanism. This method can analytically determine the linkage dimensions which meet the Ackermann requirement at three precision points, with non-zero error at other steering angles. The optimization routine moves the precision points around to find the optimized link lengths subjected to the applicable constraints. This chapter will illustrate the capabilities of this design tool by means of an example. The design tool has been completed using Microsoft Excel and is simple and easy to use. It provides instant results and allows for quick and easy parameter changes. It is ideally suited for iterative preliminary design. This tool has been previously documented in a publication by the author [31].

3.2 Example Problem

This example illustrates the procedure for finding an optimum steering mechanism for a student Formula One race car. Table 3.1 shows the parameters of the vehicle and Table 3.2 shows the constraints. Figure 3.1 illustrates these parameters in a top view. It is desired that the car have Ackermann steering across the whole steering range.

Table 3.1: Example parameters

Wheelbase	65	in
Trackwidth	48	in
Kingpin Width	46	in
Width R and P	13	in
Rack Ratio	3.2	in/pinion turn
ΔLg (whole range)	4	in
Phi 0	≤ 7 and ≥ -5	deg
Static Toe	1	deg
Steering Range (+/-)	25	deg
% Ackerman	100	%

Table 3.2: Example problem constraints

Constraints	**Value**	**Units**
Phi 0 $\geq$	-5	degrees
Phi 0 $\leq$	7	degrees
Y1 $\geq$	-5	inches
Y1 $\leq$	5	inches
L1 $\geq$	1	inches
L1 $\leq$	5	inches

3.2.1 Design Tool Procedure

First, the parameters and constraints are entered into the respective cells in the design tool, under the *User Settings and Results* tab. Cells that require user inputs are highlighted in blue. Screen shots of the tool can be found in Appendix A.

Second, the Solver application in Excel is brought up. The text is highlighted red for all the values that are part of the solver. The *target cell* for the solver is the *Sum of Sq. Errors (SSE)* cell. The error (or structural error) is the difference between the Ackermann function and the actual loop equations of the steering system. The target cell is set equal to the "min" selector (it is desired that the square root sum of the squared errors is a minimum). Precision Points 1 and 3 for ϕ and L_g, and *Phi 0* are the values that the solver changes. Any necessary constraints are also entered into the solver.

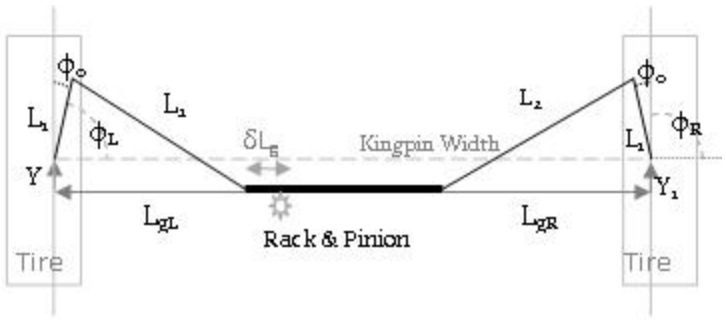

Figure 3.1: Top view of the steering system

Third, after all these parameters are input in the solver, click *solve*. Once the solver is complete, keep the solver solution. The optimized values are highlighted in yellow and are labeled: *Y1, L1,* and *L2* in the steering tool, the values for this design are shown in Table 3.3. One concern is that sometimes the solver does not find the global minimum value in the first run. It is advisable to change the precision point values to something different than the values that were used in the first run and rerun the solver. This way, if the solver did not find the global minimum the first time, it can be found by an alternate starting point. If it did find a global minimum, it should find that minimum the second time.

Table 3.3: Synthesis results

OUTPUTS		
Parameter	**Value**	**Units**
Y1	**4.999996**	inches
L1	**4.344146**	inches
L2	**19.11351**	inches

Figure 3.2 shows the structural error chart that is displayed in the tool. The tool synthesized an excellent steering system for the given design parameters and constraints. There are four points of zero standard error for both the right and left wheels in the system. The entire system is within ± 0.4 degrees of steering error from 100% Ackermann steering.

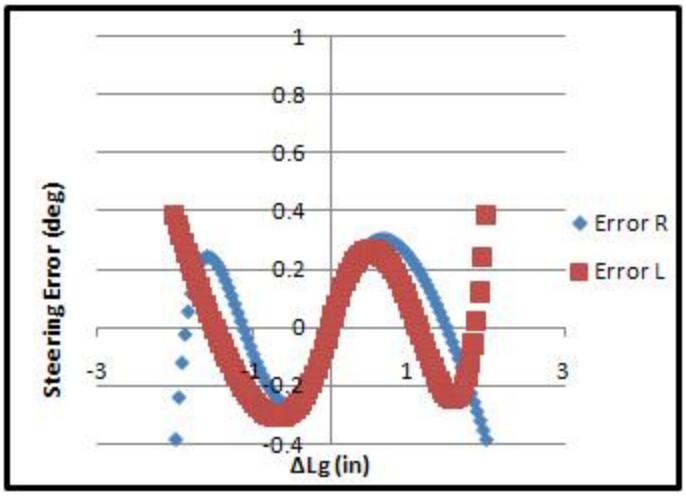

Figure 3.2: The standard error of the designed steering mechanism.

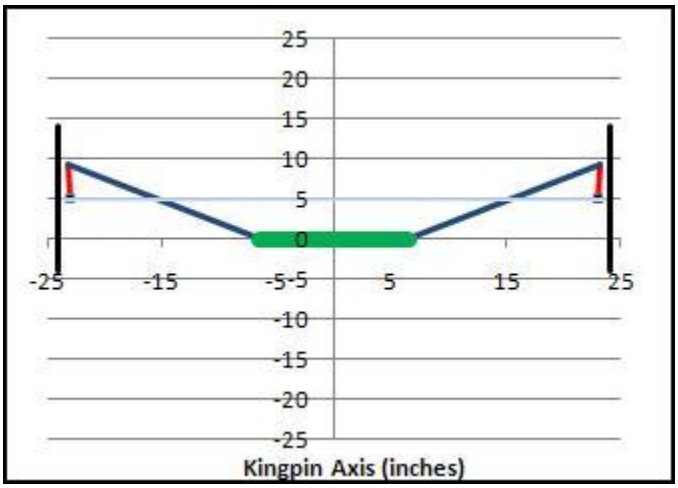

Figure 3.3: A top view of the designed steering system.

The solver only had to be run one time to find this design. Figure 3.3 shows a figure of what the minimum structural error steering system looks like (top view), at a zero steer angle.

To illustrate the importance of the solver routine, Fig. 3.4 shows the steering system structural error of a system that used the Chebychev spacing points [24] as the precision points rather than the optimized parameters. As can be seen, the system does not follow Ackermann steering as well as the optimized system.

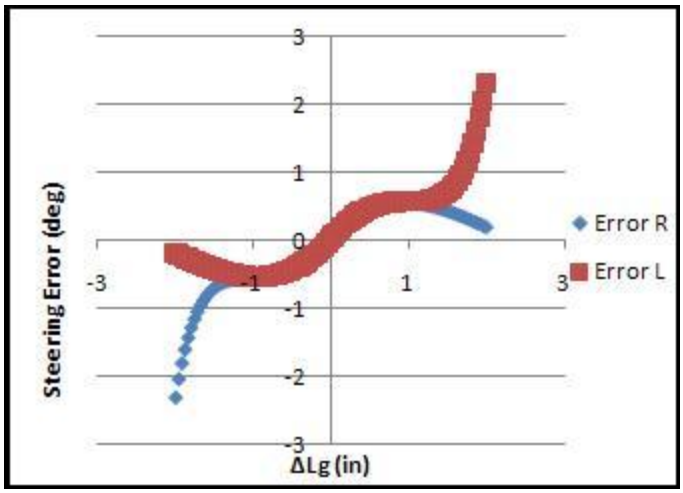

Figure 3.4: The structural error of the non-optimized steering system.

Next, the tolerances and pin clearances that are expected on the actual system can be input. These calculations are completed using the method described in Chapters 4 and 5. The method described is the Direct Linearization Method (DLM). A Taylor Series Expansion is completed on the vector loop equations (that are set out for the whole operating range of the mechanism) and tolerance sensitivities are calculated. Tolerances are obtained using a statistical root sum square method.

Once the tolerances are input, the corresponding charts are updated immediately. Table 3.4 shows the tolerances that are expected for this example. Figure 3.5 shows the structural error combined with the tolerance error (without including pin clearance errors) and Fig. 3.6 shows the structural error with the tolerance and clearance errors all combined. As can be seen in the figures, the tolerances can have drastic effects on the designed system. The tolerances do not just shift the curves up or down, they apply differently all along the range of the mechanism. This is why using the method referenced above is so powerful - it applies the tolerances realistically with the changes in geometry.

The cell *SSE - TOL - Leading* can also be the target cell for the solver. This cell value holds the sum of square errors for the structural error combined with the tolerance and clearance errors. This way, the steering system will be designed for a minimum value, with the tolerance and clearances considered.

Table 3.4: Tolerance and pin clearance values

Tolerances		
Parameter	**Value**	**Units**
Lg	0.01	inches
L1	0.008	inches
L2	0.015	inches
Y1	0.01	inches
Pin Joint Clearance		
Parameter	**Value**	**Units**
alpha1	0.02	inches
alpha2	0.02	inches
alpha3	0.02	inches

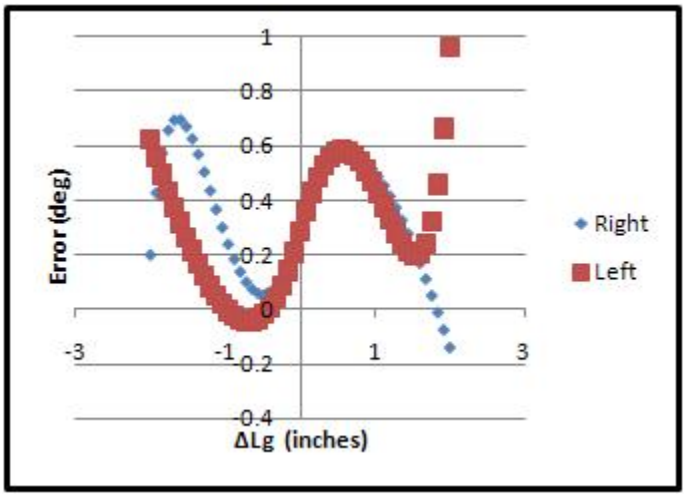

Figure 3.5: The standard and tolerance errors for the designed mechanism.

3.2.2 Design Iterations and Other Features

Suppose after all this design work has been completed, the steering team receives word from the structures team that the wheelbase and some of the constraints had to be changed. Table 3.5 shows the changed parameters. Changing the wheelbase of the vehicle is a large change that would usually require a whole new development of the steering system. With this tool, the changes can be updated and the solver rerun. In a matter of seconds, the design has been corrected to the new parameters.

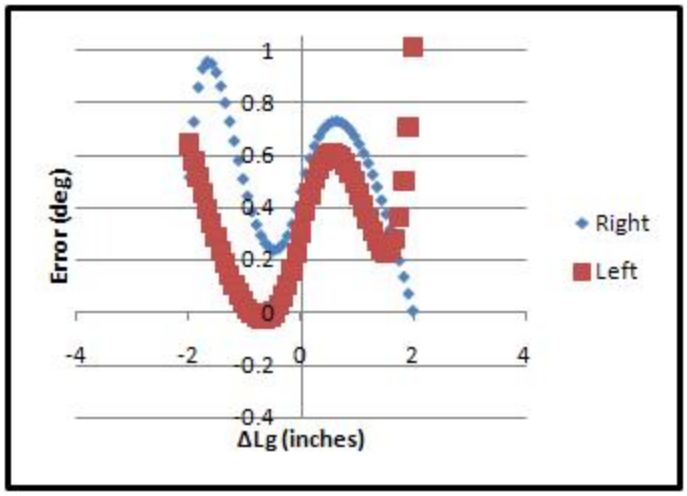

Figure 3.6: The standard, tolerance, and clearance errors for the designed mechanism.

Table 3.5: The modified example parameters

Wheelbase	62	in
Static Toe	2	deg
Steering Range (+/-)	28	deg

Figure 3.7 shows the new structural error of the system, Fig. 3.8 shows the structural error combined with the tolerance and clearance errors.

This illustrates how easy it is to change any of the parameters in the steering tool. Updates only take seconds and a new optimized steering system is synthesized. After each parameter change/adjustment, the solver must be run to re-synthesize the mechanism.

As is shown in Fig. 3.7, the second synthesized system is not quite as good as the first system. It might be wise to change a few constraints and maybe a few other parameters in order to get the system to perform a little better.

Another feature of the tool is that the Ackermann steering can be selected in percentages. Often times in racing situations, it is desirable to have less than Ackermann steering (depending on the expert that you talk to [23, 27, 28]). This can be entered in as a specified parameter.

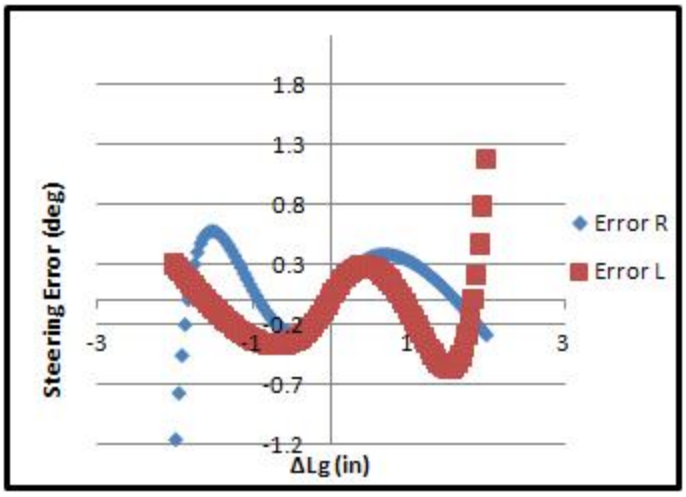

Figure 3.7: The standard error of the modified system

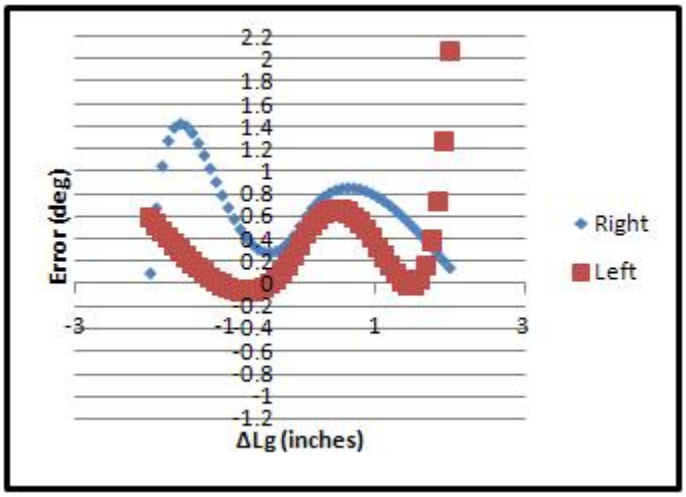

Figure 3.8: The standard, tolerance, and clearance errors for the modified mechanism.

A different worksheet tab contains another valuable tool. The *2nd System Comp.* tab provides the ability for the user to insert parameters of another steering system and compare it to the one entered into on the *User Settings and Results* tab. A chart is displayed on the 2nd System Comp. tab that compares the two designed systems, it shows the difference in steering angles.

Another useful feature is the output in the *Max Turn of Steering Wheel* cell. This value shows how many degrees the steering wheel must be turned in order for the max

turning angle on the tires to be reached. The *Steering Ratio* cell uses these results to provide the overall steering ratio of the system (how many degrees must be turned at the steering wheel for one degree of change in the tire angle). For this example and the first set of parameters, the Steering Ratio of the vehicle ends up being 9 to 1.

3.2.3 Other Configurations

The steering tool also can calculate the steering for a trailing configuration steering mechanism. It is very easy to switch between the two. The only thing that changes from the sequence above is that the target cell of the Solver is the *SSE - Trailing* cell. The constraints and other inputs are left the same as before, just click solve. The solver will optimize the system for a trailing configuration mechanism and charts with the same information as those above are shown (the top view of the system, and the structural error, without and with tolerances and joint clearances).

The steering tool can also synthesize CTO steering systems. An example of this has been completed in [24]. The only change is the length of the Rack and Pinion. A CTO linkage would only have small length for this value, like one or two inches.

3.3 Conclusions

This valuable engineering tool has been developed to help design engineers find an optimum 2-D steering mechanism quickly. It provides the capability for designers to search through different possibilities quickly and find the best solutions for the constraints that are present. It helps the designer to design leading or trailing, CTO or STO steering systems, and provides him/her with the ability to select the percentage of Ackermann steering desired, input probable tolerance or position errors, see the structural and tolerance errors displayed graphically over the steering range, and compare two different systems. The tool is very useful for designers to complete and refine preliminary designs.

Chapter 4

Variation Analysis of Position, Velocity, and Acceleration of Two-Dimensional Mechanisms by the Direct Linearization Method

4.1 Introduction

Variation analysis is typically used to verify that critical dimensions in an assembly are controlled by predicting the stack-up of contributing component variations. It is routinely used in manufacturing and assembly environments with great success. However, geometric variation not only affects critical fits and clearances in static part assemblies, it can also cause variation in mechanisms - dynamic assemblies. This chapter documents how variations in geometry cause variations in the position, velocity and acceleration performance of two-dimensional mechanisms. Huo and Chase [32] demonstrated the similarity between the velocity equation of a mechanism and it's variation in position. They found that the sensitivity matrix from the tolerance analysis was equivalent to the Jacobian matrix of the vector loop assembly model. This chapter discusses how this similarity can be extended, so that the derivative of the Jacobian matrix of the vector model may be used to describe variation in velocity and the second derivative of the Jacobian Matrix of the vector model may be used to describe variation in acceleration. Combined with statistical analysis, the variation of an entire population may be characterized without resorting to Monte Carlo simulations.

The work reported here is closed-form, using the approach described by Chase [6], called the Direct Linearization Method (DLM). This method solves for the variation (standard deviations) of assembly, or dependent variables, given the nominal (mean) values of all the variables and the tolerances of the component, or independent variables. This is a vector-loop-based assembly variation model. It uses a Taylor Series expansion to linearize

the derivatives. Each two dimensional vector loop yields three scalar equations, a summation in X, in Y, and an angular equation to sum the relative angles. In this analysis, only the equations in X and Y are used, because there are only two unknowns in each loop. Since the solutions change with geometry, variation analysis must be performed at multiple positions of the mechanism to extract data which describes the position, velocity, and acceleration variation over the full range of motion. Because this method is closed form, little computation time is needed to arrive at a solution. In fact, for the work that has been done thus far, Microsoft Excel has proven more than sufficient for all calculation and plotting. This Chapter and Chapter 5 are based on an article previously published by the author, [33].

4.2 Direct Linearization Method Applied to Mechanisms

Positional variation analysis of an assembly is completed using the DLM. A brief summary of the procedure is presented here:

1. The critical performance parameters of the assembly are identified. Equivalent kinematic mechanisms are introduced in the assembly by creating vector chains through the contributing dimensional and geometric features. For more complex mechanisms, multiple loops of vectors may be required.

2. Kinematic joints are inserted at the mating surfaces of the parts within the assembly.

3. The kinematic loops and corresponding equations are formed.

4. Partial differentials are taken with respect to the independent and dependent variables in the equivalent mechanism (the independent variables are those whose geometric variations are known, the dependent variables are assembly variations which will be found through the analysis).

5. The dependent and independent partial derivatives are grouped into corresponding matrices and solved for the dependent variables (critical assembly parameters) using linear algebra.

6. Worst case and/or statistical expressions are calculated as estimates of the variation.

This process lends itself very nicely to variation analysis of actual mechanisms. The following example will proceed through the derivation and illustrate the process.

4.2.1 Assumptions

The linearization method uses a Taylor Series expansion and truncation, step four, to approximate the derivatives - making the calculations linear. The steps that show the actual implementation of the Taylor Series in each derivation are assumed and the first terms of the partial derivatives are retained. Additional terms of the expansion are neglected for the reasons stated below.

The analysis is statistical and the errors in this work are assumed to be normally distributed, because they are induced from production. The second and third terms of the expansion refer to skewness and kurtosis, respectively, which are used to alter the normal distribution. An application of these in the DLM has been completed by Glancy [34].

The variation terms are also usually very small - the examples here use values ranging from 0.001 to 0.04. If second order terms were used, these small values would be squared, resulting in minute contributions.

4.3 Example Problem: Four-Bar Mechanism

Table 4.1: Parameters for the four-bar example problem

Variable	Value	Variation
r_1	5 cm	0.02 cm
r_2	2 cm	0.01 cm
r_3	5 cm	0.02 cm
r_4	4.5 cm	0.015 cm
θ_2	$0 to 2\pi r$	0.0017 r
ω_2	1 r/s	0.0017 r/s
α_2	0 r/s^2	0.0017r/s^2

This example analyzes a vector model of a four-bar linkage called a crank and rocker mechanism, Fig. 4.1. As the input crank, r_2, rotates a complete revolution, the output rocker oscillates. The designer sets specified limits for θ_4, ω_4, and α_4, based on application requirements. The analysis is described by a single closed vector loop. Each vector represents a link with a specified length and variation. θ_1 can arbitrarily be aligned with the X axis, so it's variation can always be eliminated. θ_2, ω_2, and α_2 are specified inputs, with probable errors on each. The nominal values of θ_3, ω_3, α_3 and θ_4, ω_4, α_4 are found using a numerical solver or by calculation. The variations of θ_3, ω_3, α_3 and θ_4, ω_4, α_4 are the unknowns sought by this method. It is assumed that the input variations are small compared to the nominal dimensions.

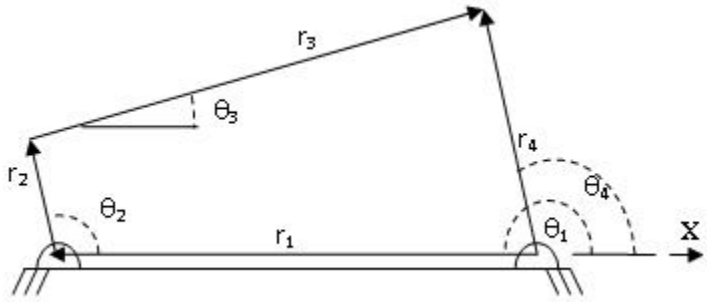

Figure 4.1: Four-bar crank and rocker mechanism

4.3.1 Position Variation Analysis

The DLM is readily applied to mechanisms. The first steps are to establish critical assembly parameters, joints, and loop equations. The critical parameters are identified above in the example introduction. The joints are the four pin joints of the mechanism. The position equation for the mechanism is described by Eqn. 4.1.

$$0 = r_1 e^{i\theta_1} + r_2 e^{i\theta_2} + r_3 e^{i\theta_3} - r_4 e^{i\theta_4} \tag{4.1}$$

A Taylor Series expansion is completed on Eqn. 4.1, retaining only the first order terms, Eqn. 4.2. This step is analogous to taking the time derivative on Eqn. 4.1, in which

case the dr and $d\theta$ terms would become velocities.

$$0 = dr_1 e^{i\theta_1} + dr_2 e^{i\theta_2} + r_2 d\theta_2 e^{i\theta_2} + dr_3 e^{i\theta_3} + r_3 d\theta_3 e^{i\theta_3} - dr_4 e^{i\theta_4} - r_4 d\theta_4 e^{i\theta_4} \tag{4.2}$$

Euler's identity is used to resolve the vectors into the x and y components.

$$e^{i\theta} = cos(\theta) + isin(\theta) \tag{4.3}$$

In step five of the DLM, all the partial derivative terms are evaluated at the nominal position of the variables and grouped into matrices (The authors used the closed form equations provided by [35] to determine the nominal angles θ_3 and θ_4 throughout the range of the mechanism). The known variations are grouped in the vector $\{\Delta X\}$ and the unknown assembly variations in $\{\Delta U\}$. In general, $\{\Delta X\}$ and $\{\Delta U\}$ could include length and angle variations. For closed loops, the partial derivatives with respect to the independent terms are placed into the [A] matrix, the dependent terms into the [B] matrix. The [B] matrix should be square. The matrix equation for the closed loops is:

$$0 = [A]\{\Delta X\} + [B]\{\Delta U\} \tag{4.4}$$

The [A] and [B] matrices and $\{\Delta X\}$ and $\{\Delta U\}$ vectors are composed as follows (the last two columns in the [A] matrix are zeros and are placeholders so the results can be substituted in the velocity and acceleration matrix analyses).

$$[A] = \begin{bmatrix} \frac{\partial H_x}{\partial r_1} & \frac{\partial H_x}{\partial r_2} & \frac{\partial H_x}{\partial r_3} & \frac{\partial H_x}{\partial r_4} & \frac{\partial H_x}{\partial \theta_2} & \frac{\partial H_x}{\partial \omega_2} & \frac{\partial H_x}{\partial \alpha_2} \\ \frac{\partial H_y}{\partial r_1} & \frac{\partial H_y}{\partial r_2} & \frac{\partial H_y}{\partial r_3} & \frac{\partial H_y}{\partial r_4} & \frac{\partial H_y}{\partial \theta_2} & \frac{\partial H_y}{\partial \omega_2} & \frac{\partial H_y}{\partial \alpha_2} \end{bmatrix} \tag{4.5}$$

$$[B] = \begin{bmatrix} \frac{\partial H_x}{\partial \theta_3} & \frac{\partial H_x}{\partial \theta_4} \\ \frac{\partial H_y}{\partial \theta_3} & \frac{\partial H_y}{\partial \theta_4} \end{bmatrix} \tag{4.6}$$

$$[\Delta X] = \{dr_1 \quad dr_2 \quad dr_3 \quad dr_4 \quad d\theta_2 \quad d\omega_2 \quad d\alpha_2\}^T \tag{4.7}$$

$$\{\Delta U\} \quad = \quad \{d\theta_3 \quad d\theta_4\}^T \tag{4.8}$$

In general, there is a third equation composed of the sum of the relative angles. However, in this case the sum vanishes identically because there are only two unknowns.

Equation 4.4 is solved for the dependent variation $\{\Delta U\}$ by linear algebra to yield Eqn. 4.9:

$$\begin{aligned} \{\Delta U\} &= \left[-[B]^{-1}[A]\right]\{\Delta X\} \\ &= [S_p]\{\Delta X\} \end{aligned} \tag{4.9}$$

The resulting -$[B]^{-1}[A]$ matrix is called the position sensitivity matrix $[S_P]$. In tolerance analysis, this is typically called the "tolerance sensitivity" matrix. The benefit of this method is that all the tolerance sensitivities are obtained with a simple matrix operation; which may be performed on a desktop computer or a scientific hand calculator.

Once the nominal values for all the angles are determined, the matrices may be evaluated using Eqn. 4.9 at each increment in angle. For reference, the sensitivity matrix is calculated in Table 4.2 for a single position at the nominal values of θ_2 = 0.698 r, θ_3 = 0.694 r, and θ_4 = 1.487 r.

Table 4.2: Position sensitivity matrix

	dr_1	dr_2	dr_3	dr_4	$d\theta_2$	$d\omega_2$	$d\alpha_2$
$d\theta_3$	-0.024	-0.198	-0.197	-0.281	-0.398	0	0
$d\theta_4$	-0.240	-0.312	-0.312	-0.219	0.002	0	0

Worst case or statistical methods may be used to estimate the variation of the dependent variables, as shown below.

Worst case:

$$\Delta U_i = \sum_{j=1}^{m} \left|S_{ij}\right| \Delta X_j \tag{4.10}$$

Statistical model:

$$\Delta U_i = \sqrt{\left(\sum_{j=1}^{m} |S_{ij}| \Delta X_j\right)^2} \tag{4.11}$$

Where i = 1, , n (number of dependent variables), $\{\Delta X\}_j$ is the tolerance of the jth (from 1 to m) independent variable, and [S] is the sensitivity matrix of the mechanism (For position, velocity or acceleration).

When parts are in production, the $\{\Delta X\}_j$ values are obtained by measuring each dimension and calculating the standard deviations. In the design stage, however, assembly variations are often estimated by substituting the dimensional tolerances for each $\{\Delta X\}_j$. Hence, designers commonly refer to this process as "tolerance analysis". When using the statistical model, the specified tolerances and each resulting $\{\Delta U\}_i$ represent $\pm 3\sigma$ variations.

Figure 4.2 and 4.3 show the nominal values and the standard deviations of the positions of θ_3 and θ_4 vs. θ_2. Clearly, the variations of θ_3 and θ_4 are not constant over the range of the mechanism. The range of position variation is informative and valuable for a designer.

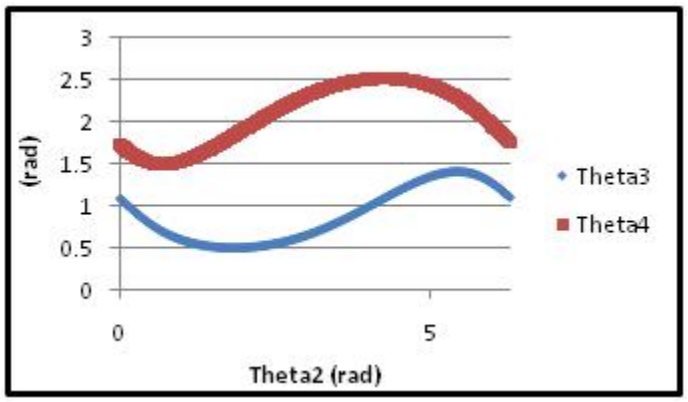

Figure 4.2: Nominal values of θ_3 and θ_4 vs. θ_2

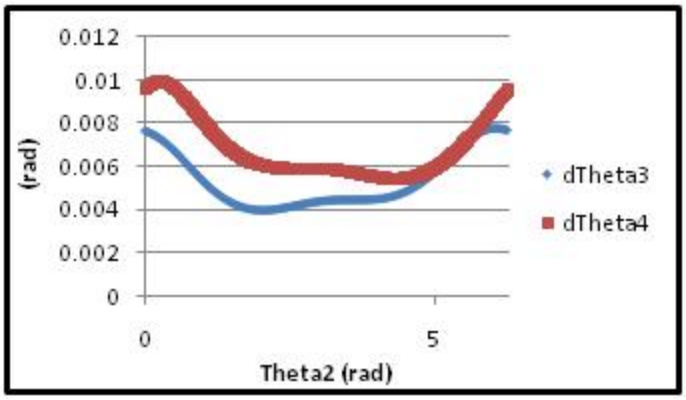

Figure 4.3: Variations of θ_3 and θ_4 vs. θ_2

4.3.2 Velocity Variation Analysis

The velocity variation analysis begins with the velocity vector equation of the mechanism:

$$0 = r_2\omega_2 ie^{i\theta_2} + r_3\omega_3 ie^{i\theta_3} - r_4\omega_4 ie^{i\theta_4} \tag{4.12}$$

The Taylor Series expansion is performed on Eqn. 4.12 with respect to each variable. This step is analogous to taking the time derivative of Eqn. 4.12, where the dr and dθ terms would become velocities and the dω terms the accelerations. Each term of Eqn. 4.12 above results in three terms of the form shown below, for a total of nine terms:

$$0 = dr_2\omega_2 ie^{i\theta_2} + r_2 d\omega_2 ie^{i\theta_2} - r_2\omega_2 d\theta_2 e^{i\theta_2} + \ldots \tag{4.13}$$

At this point, the procedure is similar to the position analysis. The vector equation is separated into an X equation and a Y equation, using Eqn. 4.3. The independent derivatives are grouped into the [C] matrix, the dependent variables for position are grouped into the [D] matrix, and the dependent variables for velocity are grouped into the [E] matrix. The [D] and [E] matrices should be square.

$$0 = [C]\{\Delta X\} + [D]\{\Delta U\} + [E]\{\Delta V\} \tag{4.14}$$

Below are the forms for the [C], [D], and [E] matrices and the $\{\Delta V\}$ vector (The last column in the [C] matrix is composed of zeros, to insert the results in the acceleration analysis).

$$[C] = \begin{bmatrix} \frac{\partial V_x}{\partial r_1} & \frac{\partial V_x}{\partial r_2} & \frac{\partial V_x}{\partial r_3} & \frac{\partial V_x}{\partial r_4} & \frac{\partial V_x}{\partial \theta_2} & \frac{\partial V_x}{\partial \omega_2} & \frac{\partial V_x}{\partial \alpha_2} \\ \frac{\partial V_y}{\partial r_1} & \frac{\partial V_y}{\partial r_2} & \frac{\partial V_y}{\partial r_3} & \frac{\partial V_y}{\partial r_4} & \frac{\partial V_y}{\partial \theta_2} & \frac{\partial V_y}{\partial \omega_2} & \frac{\partial V_y}{\partial \alpha_2} \end{bmatrix} \tag{4.15}$$

$$[D] = \begin{bmatrix} \frac{\partial V_x}{\partial \theta_3} & \frac{\partial V_x}{\partial \theta_4} \\ \frac{\partial V_y}{\partial \theta_3} & \frac{\partial V_y}{\partial \theta_4} \end{bmatrix} \tag{4.16}$$

$$[E] = \begin{bmatrix} \frac{\partial V_x}{\partial \omega_3} & \frac{\partial V_x}{\partial \omega_4} \\ \frac{\partial V_y}{\partial \omega_3} & \frac{\partial V_y}{\partial \omega_4} \end{bmatrix} \tag{4.17}$$

$$\{\Delta V\} = \{d\omega_3 \quad d\omega_4\}^T \tag{4.18}$$

Closed loop Eqn. 4.14 is solved for $\{\Delta V\}$ in Eqn. 4.19.

$$\{\Delta V\} = \left[-[E]^{-1}[C]\right]\{\Delta X\} - \left[[E]^{-1}[D]\right]\{\Delta U\} \tag{4.19}$$

However, in place of the position results being inserted directly, the sensitivity matrix from Eqn. 4.9 is inserted, as shown in Eqn. 4.20. This step permits interactions between the [C], [D], and [E] matrices before evaluating the velocity sensitivities.

$$\begin{aligned} \{\Delta V\} &= \left[-[E]^{-1}[C] + [E]^{-1}[D][B]^{-1}[A]\right]\{\Delta X\} \\ &= [S_v]\{\Delta X\} \end{aligned} \tag{4.20}$$

The velocity sensitivity matrix results from the operations in Eqn. 4.20, $[S_V]$. For this example, ω_2 = 1 rad/sec and α_2 = 0 rad/sec^2 through the whole range of the mechanism. Solutions are calculated by either the worst case (Eqn. 4.10) or statistical methods (Eqn. 4.11). For reference, the sensitivity matrix is calculated in Table 4.3 at the nominal values of θ_2 = 0.698 r, θ_3 = 0.694 r, θ_4 = 1.487 r, ω_2 = 1 r/s, ω_3 = -0.398 r/s, and ω_4 = 0.002 r/s.

Figures 4.4 and 4.5 show the nominal (mean) and variations ($\pm 3\sigma$) of the angular velocities of ω_3 and ω_4 versus the input θ_2, moving at a constant angular velocity.

Table 4.3: Velocity sensitivity matrix

	dr_1	dr_2	dr_3	dr_4	$d\theta_2$	$d\omega_2$	$d\alpha_2$
$d\omega_3$	0.010	-0.121	0.158	0.111	0.552	-0.398	0
$d\omega_4$	0.015	0.125	0.123	0.174	0.871	0.002	0

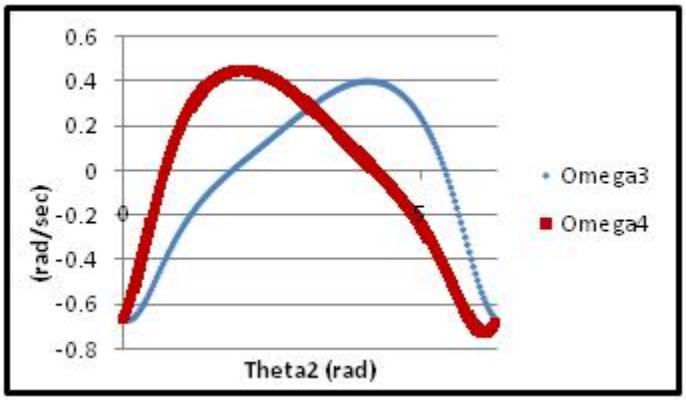

Figure 4.4: Nominal values of ω_3 and ω_4 vs. θ_2

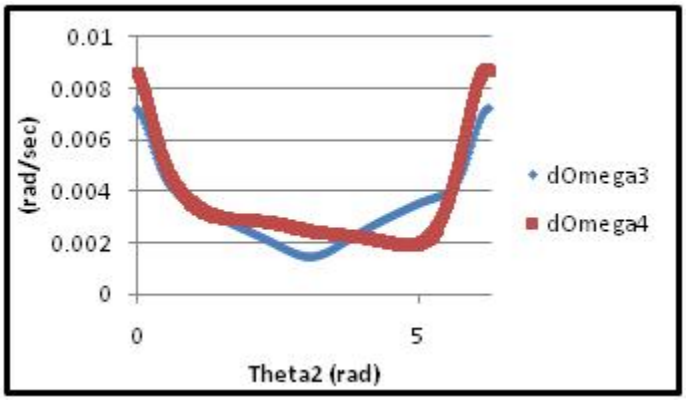

Figure 4.5: Variations of ω_3 and ω_4 vs. θ_2

4.3.3 Acceleration Variation Analysis

The vector acceleration equation for the four-bar linkage is shown below.

$$0 = r_2\alpha_2 ie^{i\theta_2} - r_2\omega_2^2 e^{i\theta_2} + r_3\alpha_3 ie^{i\theta_3} - r_3\omega_3^2 e^{i\theta_3} - r_4\alpha_4 ie^{i\theta_4} + r_4\omega_4^2 e^{i\theta_4} \tag{4.21}$$

The Taylor Series expansion is performed on Eqn. 4.21 with respect to all the variables and the first order terms are kept (only the expansion of the first two terms of Eqn. 4.21 is shown below). Equation 4.22 is analogous to taking the time derivative of Eqn. 4.21, in which case each dr and dθ would become a velocity, each dω would become an acceleration, and each dα would become a jerk.

$$\begin{aligned} 0 = {} & dr_2\alpha_2 ie^{i\theta_2} + r_2 d\alpha_2 ie^{i\theta_2} - r_2\alpha_2 d\theta_2 e^{i\theta_2} \\ & -dr_2\omega_2^2 e^{i\theta_2} - 2r_2\omega_2 d\omega_2 e^{i\theta_2} - r_2\omega_2^2 d\theta_2 ie^{i\theta_2} \end{aligned} \tag{4.22}$$

Equation 4.3 is used to extract the X and Y components from Eqn. 4.22. The terms are then grouped into matrices: independent variables are grouped into the [G] matrix, the position dependent variables into the [H] matrix, the velocity dependent variables into the [I] matrix, and the acceleration dependent variables into the [J] matrix. Eqn. 4.23 is the matrix equation that describes the acceleration variation, $\{\Delta W\}$.

$$0 = [G]\{\Delta X\} + [H]\{\Delta U\} + [I]\{\Delta V\} + [J]\{\Delta W\} \tag{4.23}$$

The forms for the [G], [H], [I], and [J] matrices and the $\{\Delta W\}$ vector are below.

$$[G] = \begin{bmatrix} \frac{\partial W_x}{\partial r_1} & \frac{\partial W_x}{\partial r_2} & \frac{\partial W_x}{\partial r_3} & \frac{\partial W_x}{\partial r_4} & \frac{\partial W_x}{\partial \theta_2} & \frac{\partial W_x}{\partial \omega_2} & \frac{\partial W_x}{\partial \alpha_2} \\ \frac{\partial W_y}{\partial r_1} & \frac{\partial W_y}{\partial r_2} & \frac{\partial W_y}{\partial r_3} & \frac{\partial W_y}{\partial r_4} & \frac{\partial W_y}{\partial \theta_2} & \frac{\partial W_y}{\partial \omega_2} & \frac{\partial W_y}{\partial \alpha_2} \end{bmatrix} \tag{4.24}$$

$$[H] = \begin{bmatrix} \frac{\partial W_x}{\partial \theta_3} & \frac{\partial W_x}{\partial \theta_4} \\ \frac{\partial W_y}{\partial \theta_3} & \frac{\partial W_y}{\partial \theta_4} \end{bmatrix} \tag{4.25}$$

$$[I] = \begin{bmatrix} \frac{\partial W_x}{\partial \omega_3} & \frac{\partial W_x}{\partial \omega_4} \\ \frac{\partial W_y}{\partial \omega_3} & \frac{\partial W_y}{\partial \omega_4} \end{bmatrix} \tag{4.26}$$

$$[J] = \begin{bmatrix} \frac{\partial W_x}{\partial \alpha_3} & \frac{\partial W_x}{\partial \alpha_4} \\ \frac{\partial W_y}{\partial \alpha_3} & \frac{\partial W_y}{\partial \alpha_4} \end{bmatrix} \tag{4.27}$$

$$\{\Delta W\} = \{d\alpha_3 \quad d\alpha_4\}^T \tag{4.28}$$

Equation 4.29 is the solution of Eqn 4.23 for $\{\Delta W\}$:

$$\{\Delta W\} = -[J]^{-1}[G]\{\Delta X\} - [J]^{-1}[H]\{\Delta U\} - [J]^{-1}[I]\{\Delta V\} \tag{4.29}$$

Equation 4.30 shows the terms from the previous analyses (Eqns. 4.9 and 4.20) substituted into Eqn. 4.29:

$$\begin{aligned} \{\Delta W\} &= \Big[-[J]^{-1}[G] + [J]^{-1}[H][B]^{-1}[A] \\ &\quad + [J]^{-1}[I][E]^{-1}[C] - [J]^{-1}[I][E]^{-1}[D][B]^{-1}[A]\Big]\{\Delta X\} \\ &= [S_A]\{\Delta X\} \end{aligned} \tag{4.30}$$

Equation 4.30 results in the acceleration sensitivity matrix, $[S_A]$. It is combined with the equation for worst case (Eqn. 4.10) or statistical methods (Eqn 4.11) to estimate the variations in acceleration, evaluated at increments along the mechanism's range. The acceleration sensitivity matrix is shown in Table 4.4, calculated at the nominal input values of θ_2 = 0.698 r, θ_3 = 0.694 r, θ_4 = 1.487 r, ω_2 = 1 r/s, ω_3 = -0.398 r/s, ω_4 = 0.002 r/s, $\alpha_2 = 0r/s^2$, $\alpha_3 = 0.552r/s^2$, and $\alpha_4 = 0.871r/s^2$.

Table 4.4: Acceleration sensitivity matrix

	dr_1	dr_2	dr_3	dr_4	$d\theta_2$	$d\omega_2$	$d\alpha_2$
$d\alpha_3$	0.250	0.521	0.113	0.079	-0.024	0.979	-0.398
$d\alpha_4$	0.190	0.598	0.127	-0.192	-0.568	1.547	0.002

Figures 4.6 and 4.7 show nominal (mean) and the variations ($\pm 3\sigma$) in the angular accelerations of α_3 and α_4, vs. θ_2. The chart of the nominal accelerations shows that the peak accelerations occur at the zero points of the velocity - as expected. The magnitudes of the peaks are important in determining max dynamic bearing loads and unbalanced forces. The variation chart shows that the greatest variations in acceleration occur at the points of maximum nominal acceleration - which could significantly affect the peak dynamic forces.

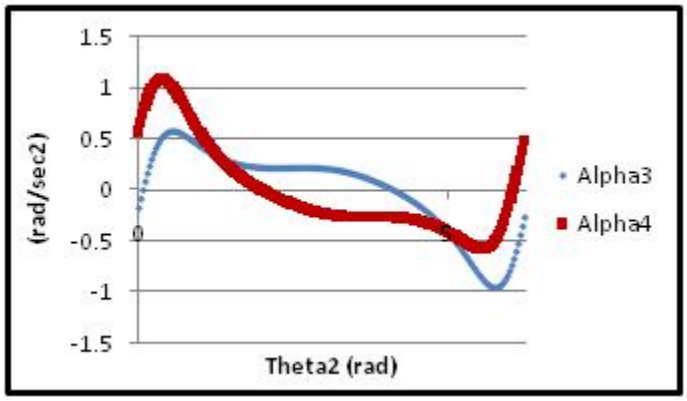

Figure 4.6: Nominal values of α_3 and α_4 vs. θ_2

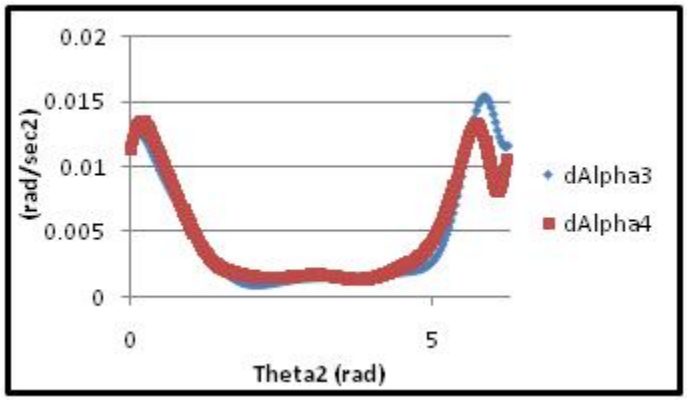

Figure 4.7: Variations of α_3 and α_4 vs. θ_2

4.3.4 Percent Contributions

This example has illustrated that small changes in dimension do contribute variation in the higher order kinematic terms for a mechanism. The variations are not constant along the mechanism range - even when the mechanism is being driven at a constant velocity. When a mechanism is required to have precise kinematic performance, the variations in the physical dimensions need to be taken into account to verify that the mechanism will be able to perform as required.

A thorough investigation would include calculations of the percent contribution, Eqn. 4.31, of each dimensional variable at the critical points along the range of the mechanism. S_{ij} is the sensitivity matrix (either for position, velocity, or acceleration), ΔX_j is the variation of the parameter that is being examined, and the denominator is the sum of the i^{th} sensitivity matrix row multiplied by the variation vector $\{\Delta X\}$ squared.

$$\%C_j = \frac{\left(S_{ij}\Delta X_j\right)^2}{\left(\sum_{j=1}^{m} \left|S_{ij}\right| \{\Delta X\}_j\right)^2} \tag{4.31}$$

This is important for determining which dimensions have the most effect on the variation. By controlling those values that have the greatest influence, the variation in the mechanism may be minimized effectively.

A chart of the percent contributions for position, velocity, and acceleration variations is shown in Fig. 4.8. For this chart, the position, velocity, and acceleration percent contributions all are evaluated at different θ_2 positions. $\theta_2 = 240^o$ for the position percent contribution, $\theta_2 = 178^o$ for the velocity, and $\theta_2 = 22^o$ for the acceleration. This way, critical points in all three areas can be viewed at the same time, since when acceleration is at a critical point, velocity and position are not, etc. The values for the variations at those points are: $\theta_4 = \pm 0.005$ r, $\omega_4 = \pm 0.0024$ r/s, and $\alpha_4 = \pm 0.012\, r/s^2$, as shown in the legend. The dimensional variation in the links, especially in links 2, 3, and 4, has a great effect on the output crank variation.

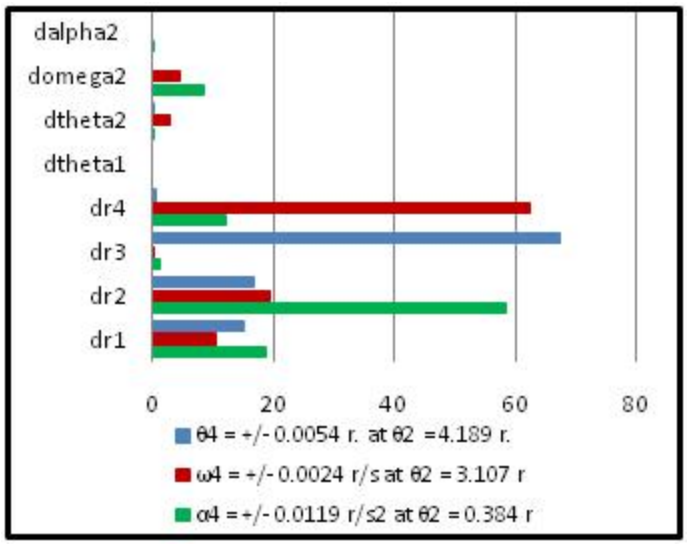

Figure 4.8: Percent contributions at certain points for position, velocity, and acceleration

4.4 Conclusion

A new method for variation analysis of assemblies has been developed for predicting the kinematic performance of 2-D mechanisms, known as the kinematic DLM. It is comprehensive. It may be applied to open and/or closed loop mechanisms. Although open loops were not exhibited in this chapter, they may be incorporated using inverse kinematics and the equations established in reference [6]. The method predicts the effects of dimensional variations on critical position, velocity, and acceleration requirements over the full range of motion of the mechanism. It is extendable to 3-D mechanisms and higher time derivative motions.

The method is efficient. The closed form statistical solution eliminates the need to simulate large numbers of assemblies with random errors and analyze them one-by-one, and to repeat the simulation at each position of the mechanism. The solution is also statistical. An entire population of assemblies may be characterized with only two solutions at each position of the mechanism: one for the mean dimensions and one for the variation about the mean.

This is a powerful new tool for mechanism designers. It is suitable for design iteration for optimized performance, and for estimating the probability of design realization.

The following chapter extends the method further by including geometric feature variations in the analysis. The geometric feature variations can be used to describe the variation that mechanism joints introduce in a mechanism.

Chapter 5

Geometric Feature Variations Applied to Mechanisms

5.1 Introduction

Chapter 4 discussed how the DLM can be applied to predict the effects of dimensional variations on the kinematics of mechanisms. A valuable extension to the kinematic DLM comes from including the effects of geometric feature variations. Geometric feature variations, such as roundness, flatness, runout, parallelism, etc., can accumulate statistically and propagate kinematically in assemblies just like dimensional variations. This fact is illustrated by Fig. 5.1, taken from [9]. This figure shows how different geometric feature variations propagate and that they actually propagate in the kinematically constrained directions at the point of contact; i.e. the cylinder on the plane has variations in the vertical direction and the block on the plane has rotational variation. The geometric feature varaions are independent of length and angular variations and are applied to contacting surfaces in an assembly. When parts contact, geometric feature variations can be applied to characterize the variations that occur [9, 10].

In mechanisms, parts contact at the joints. Accumulated variation propagates through each joint type uniquely. Five types of joints are commonly used in two-dimensional mechanisms: planar, cylinder slider, edge slider, pin, and parallel cylinder. For a majority of mechanisms, this is an advantage, because joint variations can easily be included in the vector model of a mechanism.

Geometric feature variations may be inserted at each joint in the mechanism model to account for contact variations within types of joints. Principally in mechanism analysis, feature variations may be used to include clearance in pin joints. However, there are other sources of variation introduced in other joint types that can also be taken into account.

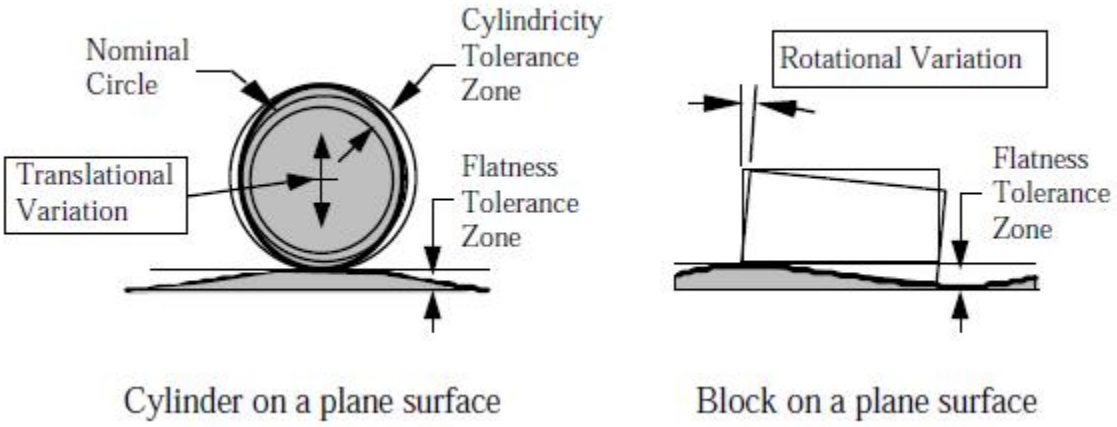

Figure 5.1: How geometric feature variations propagate kinematically

Chase [9] discusses the distinct types of variation which occur in common 2-D joints due to geometric feature variations. In summary, Fig. 5.1 shows which types of variation (rotational - R or translational - T) can occur in each 2-D joint type, due to each feature variation.

Joints \ Geom Tol	▱	—	○	⌓	⌓	//	⊥	∠	↗↗	◎	⌖
Planar	R	R			R	R	R	R	R T	R T	
Cyl Slider	T	T	T	T	T	T	T	T	T		
Edge Slider	T	T	T	T	T	T	T	T	T	T	T
Revolute										T	T
Par Cylind		T	T	T	T				T		

Figure 5.2: Variations resulting from feature variations exhibited in each 2D joint type

5.2 Example: Crank-Slider Mechanism

The application of geometric feature variations to describe variations in position, velocity, and acceleration of mechanism is illustrated through the following example.

Table 5.1: Parameters for the crank-slider example problem

Variable	Nominal	Variation
r_1	2 cm	0.01 cm
r_2	5 cm	0.03 cm
r_3	9 cm	0.04 cm
δ_1	0	0.0025 cm
δ_2	0	0.005 cm
δ_3	0	0.005 cm
δ_4	0	0.005 cm
β_4	0	0.0025 cm
θ_2	0 to 2π r	0.0017 r
ω_2	1 r/s	0.0017 r/s
α_2	0 r	$0.0017 r/s^2$

This example uses a vector model of a crank-slider mechanism, Fig. 5.2. A crank-slider mechanism is a common device used in many machines, from auto engines to electric razors. The rotating crank, r_2, drives the connecting rod, r_3, which makes the slider oscillate along r_4. The piston centerline is offset a distance r_1 from the drive-shaft. Significant variations in position, velocity, and acceleration of the piston may occur as a result of dimensional and geometric feature variations. Specified limits on the stroke, peak velocity, and peak acceleration would be set by design requirements, such as the piston clearance at top dead center, bearing forces, and balancing requirements.

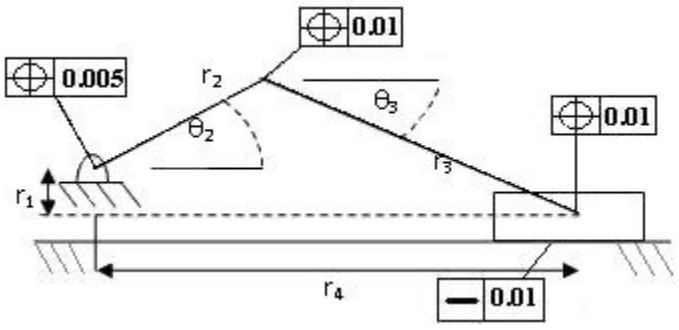

Figure 5.3: Crank-slider mechanism

The vector model of the assembly is completed using one closed loop. Each vector represents a link with a specified length and variation. r_4 can arbitrarily be aligned with the X axis and r_1 can be aligned with the Y axis, so variation in θ_1 and θ_4 can always be eliminated. θ_2, ω_2, and α_2 are specified inputs with probable errors. The nominal values of θ_3, ω_3, α_3 and r_4, v_4, a_4 are found using a numerical solver or by calculation. The variations of θ_3, ω_3, α_3 and r_4, v_4, a_4 are the unknowns found using this method. Again, it is assumed that the variations are small compared to the nominal dimensions.

Also in this example, four geometric feature variations have been included, indicated by the feature control blocks in Fig. 5.2. The first three are true position tolerances that account for random pin location due to clearance in the three pin joints. The fourth is a straightness feature on the surface where the slider contacts. Figure 5.1 above, shows that for a revolute (pin) joint, a true position feature adds translational variation; so two variation vectors are inserted at each joint - one in the horizontal and the other in the vertical direction. The δ values reported in Table 5.1 are the diameters of the tolerance zones. According to ANSI Y 14.5 standards, position tolerances represent the diameter of the tolerance zone divided by two, thus $\pm\delta/2$ is used in the calculations. For the planar joint with a straightness feature, rotational variation is added due to surface waviness and translational variation is added to illustrate how both types of variation could be incorporated in one joint (for example purposes). The rotational variation, β, is approximated following Eqn. 13 in [9], and is reproduced here, Eqn. 5.1 for reference. The characteristic length is the length of the piston, 4.0 inches in this example.

$$\pm\beta = arctan\left(\frac{\frac{\pm\delta}{2}}{characteristic\,length}\right) \tag{5.1}$$

5.2.1 Position Variation Analysis

The first step is to determine the position equation, including the geometric feature variation terms. The geometric variation terms are inserted as vectors in the x and y directions. Eqn. 5.2 shows the closed loop position equation. Note that the nominal values of

the position tolerance zones are zero, so the nominal equation actually is unchanged.

$$\begin{aligned} 0 = {} & r_1 e^{i\theta_1} + \delta_1 e^{i0} + \delta_1 e^{i\frac{\pi}{2}} + r_2 e^{i\theta_2} + \delta_2 e^{i0} + \delta_2 e^{i\frac{\pi}{2}} \\ & + r_3 e^{i\theta_3} + \delta_3 e^{i0} + \delta_3 e^{i\frac{\pi}{2}} - r_4 e^{i(\theta_4+\beta_4)} + \delta_4 e^{i\frac{\pi}{2}} \end{aligned} \tag{5.2}$$

A Taylor Series expansion is performed on Eqn. 5.2, with respect to each of the variables. Only the first terms are kept for the analysis. This step is comparable to taking the time derivative of Eqn. 5.2, where each of the delta terms would become velocities.

$$\begin{aligned} 0 = {} & dr_1 e^{i\theta_1} + d\delta_1 e^{i0} + d\delta_1 e^{i\frac{\pi}{2}} + dr_2 e^{i\theta_2} + r_2 d\theta_2 i e^{i\theta_2} + d\delta_2 e^{i0} + d\delta_2 e^{i\frac{\pi}{2}} + dr_3 e^{i\theta_3} \\ & + r_3 d\theta_3 i e^{i\theta_3} + d\delta_3 e^{i0} + d\delta_3 e^{i\frac{\pi}{2}} + d\delta_4 e^{i\frac{\pi}{2}} - dr_4 e^{i(\theta_4+\beta_4)} - r_4 d\beta_4 i e^{i(\theta_4+\beta_4)} \end{aligned} \tag{5.3}$$

Equation 5.3 is divided into two scalar equations, an H_x equation and an H_y equation, using Eqn. 4.3. The partials are then inserted into the [A], [B] matrices as in Chapter 4, with the variations, grouped into vectors, $\{\Delta X\}$ and $\{\Delta U\}$. The [A] and [B] matrices in Eqn. 4.5 and Eqn. 4.6 are very similar to those for this example, the only difference is that dr_4 becomes dependent and θ_4 is a constant. This is shown in the vectors $\{\Delta X\}$ and $\{\Delta U\}$ below.

$$\{\Delta X\} = \{dr_1 \quad dr_2 \quad dr_3 \quad d\theta_2 \quad d\omega_2 \quad d\alpha_2\}^T \tag{5.4}$$

$$\{\Delta U\} = \{d\theta_3 \quad dr_4\}^T \tag{5.5}$$

A new matrix [F] is added, into which the partial derivatives with respect to the geometric feature variations are placed. The variations of the geometric features are placed in a $\{\Delta\delta\}$ vector.

$$[F] = \begin{bmatrix} \frac{\partial H_x}{\partial \delta_1} & \frac{\partial H_x}{\partial \delta_2} & \frac{\partial H_x}{\partial \delta_3} & \frac{\partial H_x}{\partial \delta_4} & \frac{\partial H_x}{\partial \beta_4} \\ \frac{\partial H_y}{\partial \delta_1} & \frac{\partial H_y}{\partial \delta_2} & \frac{\partial H_y}{\partial \delta_3} & \frac{\partial H_y}{\partial \delta_4} & \frac{\partial H_y}{\partial \beta_4} \end{bmatrix} \tag{5.6}$$

$$\{\Delta\delta\} = \{d\delta_1 \quad d\delta_2 \quad d\delta_3 \quad d\delta_4 \quad d\beta_4\}^T \tag{5.7}$$

The method for obtaining the sensitivity equations is modified for this case, because of the additional [F] matrix and variation vector $[\Delta\delta]$. The closed loop matrix equation

becomes:

$$0 = [A]\{\Delta X\} + [B]\{\Delta U\} + [F]\{\Delta\delta\} \tag{5.8}$$

Equation 5.8 is solved for $\{\Delta U\}$ by Eqn. 5.9 below.

$$\begin{aligned} \{\Delta U\} &= \left[-[B]^{-1}[A]\right]\{\Delta X\} + \left[-[B]^{-1}[F]\right]\{\Delta\delta\} \\ &= [S_p]\{\Delta X\} + [S_{Fp}]\{\Delta\delta\} \end{aligned} \tag{5.9}$$

Just as in the example in Chapter 4, the nominal values of the angles and lengths are determined as θ_2 is incremented over the range of the mechanism. The set of nominal values for each position are used to evaluate the sensitivities in the $[S_p]$ and $[S_{Fp}]$ matrices. Expression for worst case or statistical variation stack-up may then be performed to find the variation in position. The worst case and statistical formulas are also changed to include both sensitivity matrices S_{ij} and S_{ik}:

Worst case:

$$\Delta U_i = \sum_{j=1}^{m} \left|S_{ij}\right| \Delta X_j + \sum_{k=1}^{p} |S_{ik}| \Delta\delta_k \tag{5.10}$$

Statistical model:

$$\Delta U_i = \sqrt{\left(\sum_{j=1}^{m} \left|S_{ij}\right| \Delta X_j\right)^2 + \left(\sum_{k=1}^{p} |S_{ik}| \Delta\delta_k\right)^2} \tag{5.11}$$

Where i = 1,..., n (number of dependent variables), ΔX_j is the tolerance/variance of the j^{th} independent variable; S_{ij} are the elements of the sensitivity matrix -$[B]^{-1}$[A] of the mechanism. S_{ik} are the elements of the sensitivity matrix -$[B]^{-1}$[F] for the k = 1,...,p geometric feature variations, $\Delta\delta_k$. Each of these expressions is evaluated for a single value of θ_2, as it is incremented over the full range of motion.

For reference, the two sensitivity matrices are calculated at the nominal values of $\theta_2 = 0.698$ r (40 deg), $\theta_3 = -0.618$ r (35.4 deg), and r_4 = 11.166 cm and are shown in Tables 5.2 and 5.3.

Table 5.2: Position sensitivity matrix

	dr_1	dr_2	dr_3	$d\theta_2$	$d\omega_2$	$d\alpha_2$
$d\theta_3$	-0.136	-0.088	0.079	-0.522	0	0
dr_4	-0.711	0.309	1.227	-5.936	0	0

Table 5.3: Position geometric feature sensitivity matrix

	$d\delta_1$	$d\delta_2$	$d\delta_3$	$d\delta_4$	$d\beta_4$
$d\theta_3$	-0.136	-0.136	-0.136	-0.136	1.522
dr_4	0.289	0.289	0.289	-0.711	7.936

Figures 5.4 and 5.5 show nominal (mean) and variations ($\pm 3\sigma$) in the positions of θ_3 and r_4, vs. θ_2. The largest variations in Fig. 5.5 occur at the peaks in Fig. 5.4. The variation plot is more varied because of the interaction between the two types of variation.

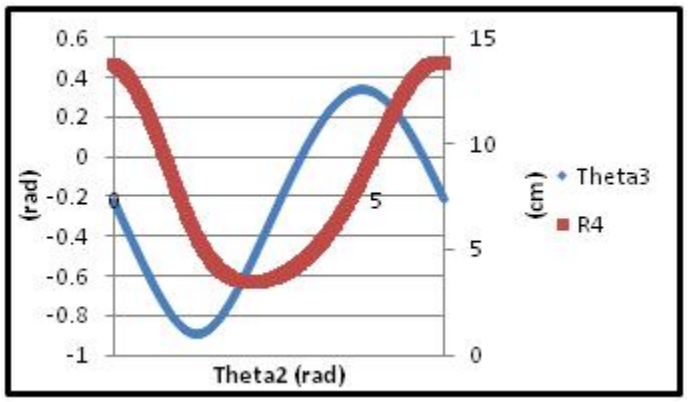

Figure 5.4: Nominal values of θ_3 and r_4 vs. θ_2

5.2.2 Velocity Variation Analysis

The velocity variation analysis, including geometric feature variation, is very similar to the analysis without geometric feature variations. The [C], [D], and [E] matrices are composed in the same way as they were for the example in Chapter 4, Eqn. 4.14 and

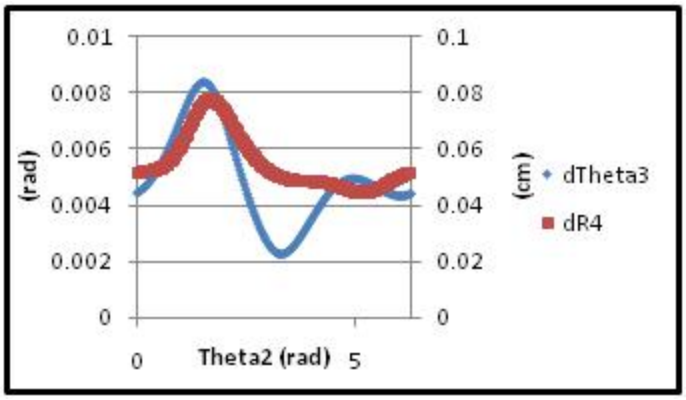

Figure 5.5: Variations of θ_3 and r_4 vs. θ_2

Eqn. 4.19. The difference is the equation used to solve for the dependent variation. Geometric variations do not appear in the velocity equation, but they are introduced by inserting the matrices for $\{\Delta U\}$ from the position analysis, Eqn. 5.9, shown in Eqn. 5.12.

$$\begin{aligned} \{\Delta V\} &= \left[-[E]^{-1}[C]+[E]^{-1}[D][B]^{-1}[A]\right]\{\Delta X\} \\ &\quad -\left[[E]^{-1}[D][B]^{-1}[F]\right]\{\Delta\delta\} \\ &= [S_v]\{\Delta X\}+[S_{Fv}]\{\Delta\delta\} \end{aligned} \tag{5.12}$$

Here it can be seen that feature variations do affect the variation in the velocity of the mechanism. The two sensitivity matrices are evaluated throughout the mechanism range and can be solved using Eqn. 5.10 or 5.11 for the dependent velocity variation. For reference, the two sensitivity matrices are calculated at the nominal values of $\theta_2 = 0.698$ r, $\theta_3 = -0.618$ r, and r_4 = 11.166 cm., ω_2 = 1 r/s, ω_3 = -0.522 r/s, and v_4 = -5.936 cm/s and are shown in Tables 5.4 and 5.5.

Table 5.4: Velocity sensitivity matrix

	dr_1	dr_2	dr_3	$d\theta_2$	$d\omega_2$	$d\alpha_2$
$d\omega_3$	-0.051	-0.137	0.087	0.244	-0.522	0
dv_4	-0.786	-1.692	0.455	-4.556	-5.936	0

Table 5.5: Velocity geometric feature sensitivity matrix

	$d\delta_1$	$d\delta_2$	$d\delta_3$	$d\delta_4$	$d\beta_4$
$d\omega_3$	-0.051	-0.051	-0.051	-0.051	0.565
dv_4	-0.786	-0.786	-0.786	-0.786	8.775

Figures 5.6 and 5.7 show nominal (mean) and variations ($\pm 3\sigma$) in the velocities of ω_3 and v_4, vs. θ_2. The peak variations occur at the peak values of velocity.

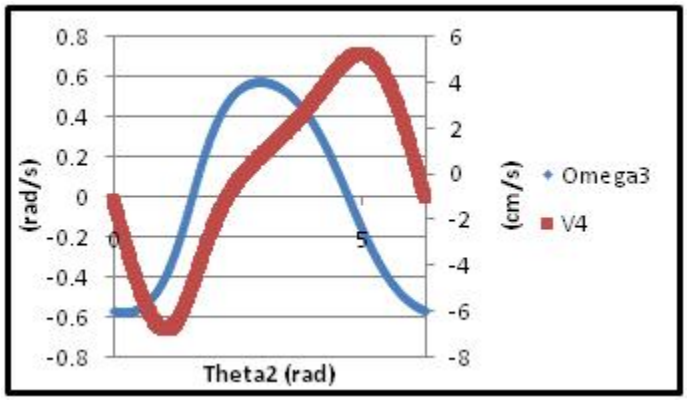

Figure 5.6: Nominal values of ω_3 and v_4 vs. θ_2

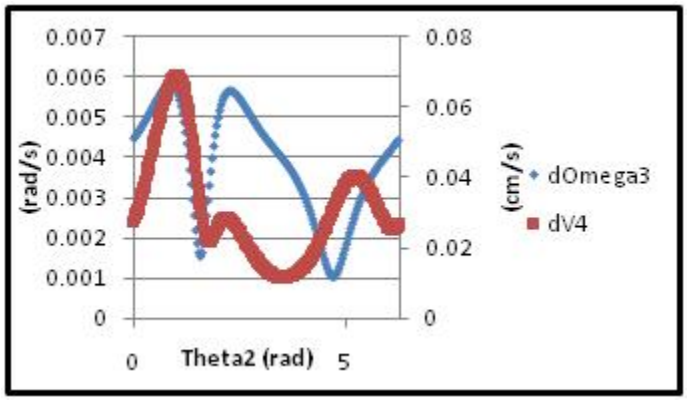

Figure 5.7: Variations of ω_3 and v_4 vs. θ_2

5.2.3 Acceleration Variation Analysis

Similar to velocity, the changes for the acceleration variation analysis are the sensitivity equations that are formed when the position and velocity variation equations are substituted into Eqn. 4.29; the result is Eqn. 5.13:

$$\begin{aligned}\{\Delta W\} &= \Big[-[J]^{-1}[G]+[J]^{-1}[H][B]^{-1}[A] \\ &\quad +[J]^{-1}[I][E]^{-1}[C]-[J]^{-1}[I][E]^{-1}[D][B]^{-1}[A]\Big]\{\Delta X\} \\ &\quad +\Big[[J]^{-1}[H][B]^{-1}[F]-[J]^{-1}[I][E]^{-1}[D][B]^{-1}[F]\Big]\{\Delta\delta\} \\ &= [S_A]\{\Delta X\}+[S\delta]\{\Delta\delta\} \end{aligned} \tag{5.13}$$

This equation is solved above using Eqns. 5.10 or 5.11, over the range of the mechanism. For reference, the two sensitivity matrices are in Tables 5.6 and 5.7; calculated at the nominal values of $\theta_2 = 0.698$ r, θ_3 = -0.618 r, and r_4 = 11.166 cm., ω_2 = 1 r/s, ω_3 = -0.522 r/s, v_4 = -5.936 cm/s, $\alpha_2 = 0\ r/s^2$, $\alpha_3 = 0.244\ r/s^2$, and a_4 = -4.556 cm/s^2.

Table 5.6: Acceleration sensitivity matrix

	dr_1	dr_2	dr_3	$d\theta_2$	$d\omega_2$	$d\alpha_2$
$d\alpha_3$	-0.051	-0.023	0.024	0.652	0.489	-0.522
da_4	-0.215	-1.652	0.459	10.162	-9.112	-5.936

Table 5.7: Acceleration geometric feature sensitivity matrix

	$d\delta_1$	$d\delta_2$	$d\delta_3$	$d\delta_4$	$d\beta_4$
$d\alpha_3$	-0.051	-0.051	-0.051	-0.051	0.570
da_4	-0.215	-0.215	-0.215	-0.215	2.406

Figures 5.8 and 5.9 show nominal (mean) and variations ($\pm 3\sigma$) in the accelerations of α_3 and a_4, vs. θ_2. The peak values of variation occur at the maximum accelerations. The values vary more because of the interaction between the two types of variation.

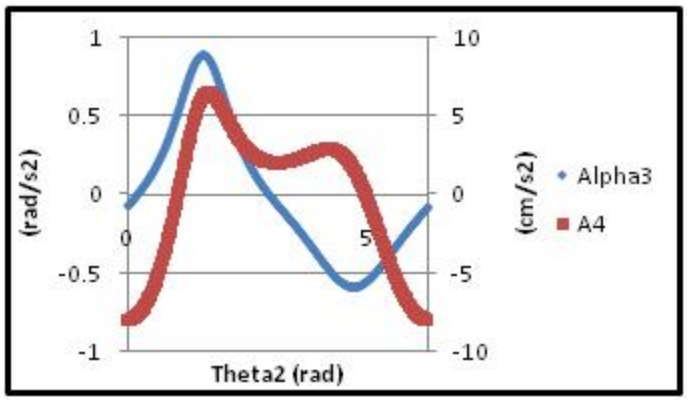

Figure 5.8: Nominal values of α_3 and a_4 vs. θ_2

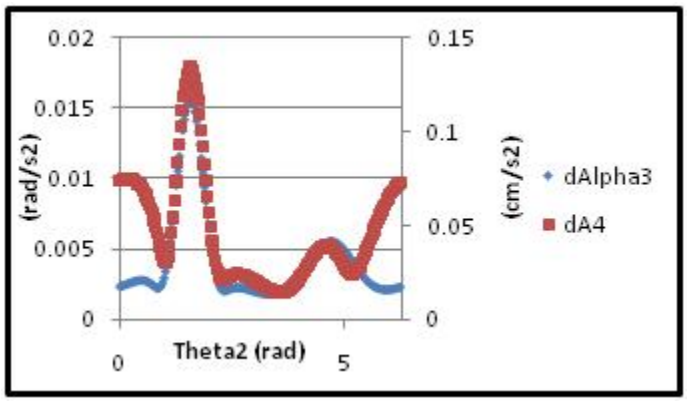

Figure 5.9: Variations of α_3 and a_4 vs. θ_2

5.3 Summary of Results

As in the example in Chapter 4, the percent contribution charts are useful in determining the major sources of variation. For this example, there are only two contributions shown; those from the dimensional and input variations and those from the geometric feature variations. Figure 5.10 shows the contributions for position, velocity, and acceleration all at the Peak Stroke ($\theta_2 = 352^o$). The percentage values will change over the range of the mechanism. At some points, most of the variation will be from length and angle variations, at others it will be mostly due to geometric feature variations, but most of the time it is mixed. While observing the percent contribution figures, it is important to remember that the magnitudes of geometric feature variations were much smaller than the dimensional

variations. Nevertheless, as is shown in Figure 5.10, the geometric feature variations still can contribute a significant amount of the total variation. This is true for position, velocity, and acceleration. Therefore, for an accurate estimation of the variation in the system, geometric feature variations must be included in the analysis.

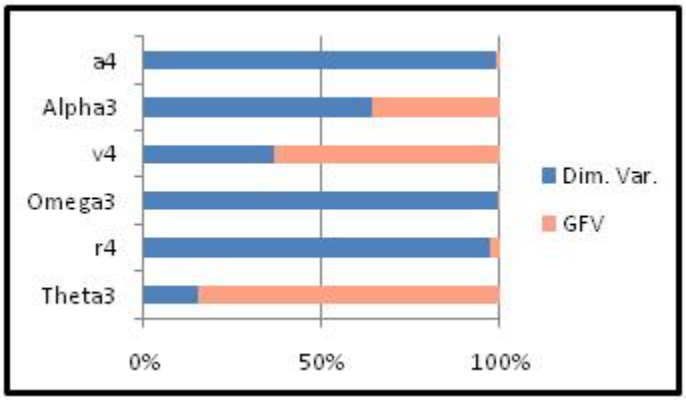

Figure 5.10: Percent contributions of dimensional and geometric feature variations at $\theta_2 = 352^o$

5.4 Conclusion

The DLM, used for variation analysis of assemblies and mechanisms, has been successfully extended by adding the variations contributed by geometric feature variations. Geometric feature variations may be added into the analysis in order to model variations that occur in kinematic joints. The joint variations do cause variations in the velocity and acceleration of critical parameters, even though they are only physically added into the position vector loops.

Chapter 6

Conclusions and Recommendations

The purpose of this research has been to extend tolerance analysis methods to dynamic mechanisms - specifically in automotive applications. This chapter reviews how the research objectives were met, discusses conclusions that can be drawn, and documents recommendations for ways in which this research can be expanded.

6.1 Research Objectives Accomplished

The research objectives that were discussed in Chapter 1 are repeated here, along with discussion of how they were accomplished.

6.1.1 Objectives - Steering

The objectives of the steering system research is to create an easy-to-use design and analysis tool with the following capabilities:

1. "Use the tool to synthesize either leading or trailing, CTO or STO steering system configurations." The equations for leading and trailing, CTO and STO configurations were developed and incorporated into the steering design tool.

2. "Provide optimization to quickly and efficiently converge to the best possible solution given multiple constraints." The completed steering system design tool utilizes the solver program to vary the parameters of the Freudenstein's equation to find optimal solutions. The system converges very quickly and allows constraints on any of the link lengths.

3. "Ability to see the effects of tolerances and pin clearances on the design." The steering tool utilizes the methods developed in Chapters 4 and 5 to provide the influences of dimensional and geometric variations and joint clearances on the designed system.

4. "Ability to adjust the percentage of Ackermann steering." The tool was developed with this capability - which provides for the needs of race car designers of designing the system to different performance goals.

5. "Visually display the structural error of the system and how tolerances affect that error throughout the range of the steering angle." Charts that show the results for a specific design, illustrate the structural error and the influences from tolerances and clearances. The charts help the designer to understand where the steering will be most accurate in meeting the Ackermann requirements.

6.1.2 Objectives - Suspension

The objectives for the suspension portion of the research are to:

1. "Build on the DLM by providing the capability to analyze the variations in position, velocity, and acceleration of any open or closed loop 2D mechanism." The DLM was effectively extended to handle mechanisms and the higher order kinematic terms. The method did not have to be drastically changed in order to provide this capability. An example was used to illustrate how this can be done.

2. "Add the capability to describe the effects of geometric feature variations on the variations of position, velocity, and acceleration of any open or closed loop 2D mechanism." By using the geometric feature variations, it was shown that variation in joints could be effectively modeled. This is a valuable capability that provides modeling of variation that cannot be "calibrated out".

6.2 Conclusions

The research put forth in this thesis has advanced the understanding of how to more fully integrate tolerance analysis capabilities into kinematic assemblies (mechanisms). Tools

necessary to apply the principles of static variation analysis to kinematic assemblies were developed. Suspension and steering systems are dynamic assemblies with critical requirements, where small changes in dimension can cause dramatic changes in the vehicle performance capabilities. Through the developed tools, suspension and steering systems can be analyzed over a range of positions to quantitatively determine the effect of small changes in dimension and geometry on the performance of that system. The tools that have been developed will also aid future research that can provide particular capabilities for automobile steering and suspension systems.

6.3 Recommendations for Future Research

1. The steering tool is only valid for planar systems. Many steering systems have inclined kingpin axes and camber. A 3D synthesis tool would be valid for much more than preliminary and simple designs. Other aspects such as bump steer and roll steer might also be incorporated into the tool.

2. The steering tool would benefit greatly by adding the capability to take into account tire loads and slip angles. This information is essential for vehicles traveling and cornering at high speeds, as it changes the objectives of the steering system substantially, [28].

3. A complete DLM has been developed for 3D static assemblies. It should be possible to demonstrate that the methods developed here for 2D mechanisms could be readily applied to 3D mechanisms. This would make the method valuable and applicable for mechanisms as complex as automobile suspension systems.

4. The work that has been done on mechanism variation could also be extended in a manner similar to the work done by Faerber [11] and Dabling [12]. Kinematic packages could then be used to analyze a mechanism and the effects of variation on that mechanism's position, velocity, and acceleration - including the effects of geometric feature variations. Mechanisms could more easily be designed to minimize variation.

5. The methods developed to account for mechanism kinematic variation should be expanded to include variational effects on the equations of motion. This would permit quantitative estimates of variation in inertia forces and moments, or other internal dynamic forces in the tires and structural members. This would also provide essential performance information, especially in the area of clearances and other joint variations. The work documented in [21] should provide good guidance on how this could be accomplished.

References

[1] Zarak, C., and Townsend, M., 1983. "Optimal design of rack-and-pinion steering linkages." *Trans. ASME,* **105**, June, pp. 220–226.

[2] Simionescu, P., and Smith, M., 2000. "Initial estimates in the design of rack-and-pinion steering linkages." *Trans. of ASME,* **122**(6), pp. 194–200.

[3] Simionescu, P., and Beale, D., 2002. "Optimum synthesis of the four-bar function generator in its symmetric embodiment: the ackermann steering linkages." *Mech. Machine Theory,* **37**, pp. 1487–1504.

[4] Hanzaki, A. R., and Saha, S., 2009. "Kinematic and sensitivity analysis and optimization of planar rack-and-pinion steering linkages." *Mech. Mach. Theory,* **44**(1), pp. 42–56.

[5] Marler, J., 1988. "Nonlinear tolerance analysis using the direct linearization method." Ms thesis, Brigham Young University, Provo, UT 84602, December.

[6] Chase, K., Gao, J., and Magleby, S., 1995. "General 2-d tolerance analysis of mechanical assemblies with small kinematic adjustments." *J. of Design and Manufacture,* **5**, pp. 263–274.

[7] Norton, R., 1999. *Machinery: An Introduction to the Synthesis and Analysis of Mechanisms and Machines*. McGraw-Hill, New York, NY.

[8] Chase, K., Gao, J., and Magleby, S., 1998. "Generalized 3-d tolerance analysis of mechanical assemblies with small kinematic adjustments." *IIE. Transactions,* **30**(4), pp. 367–377.

[9] Chase, K., Gao, J., Magleby, S., and Sorensen, C., 1996. "Including geometric feature variations in tolerance analysis of mechanical assemblies." *IIE Transactions,* **28**, pp. 795–807.

[10] Brown, C., 1995. "Statistical models for position and profile variation in mechanical assemblies." Ms thesis, Brigham Young University, Provo, UT 84602, April.

[11] Faerber, P., 1999. "Tolerance analysis of assemblies using kineamatically derived sensitivities." Ms thesis, Brigham Young University, Provo, UT 84602, August.

[12] Dabling, J., 2001. "Incorporating geometric feature variation with kinematic tolerance analysis of 3d assemblies." Ms thesis, Brigham Young University, Provo, UT 84602, August.

[13] Wittwer, J., Chase, K., and Howell, L., 2004. "The direct linearization method applied to position error in kinematic linkages." *Mechanism and Machine Theory,* **39**(7), pp. 681–693.

[14] Choi, J., Lee, S., and Choi, D., 1998. "Stochastic linkage modeling for mechanical error analysis of planar mechanisms." *Mechanics Based Design of Structures and Machines,* **26**(3), pp. 257–276.

[15] Kyung, M., and Sacks, E., 2003. "Nonlinear kinematic tolerance analysis of planar mechanical systems." *Computer-Aided Design,* **35**, pp. 901–911.

[16] Ting, K., Zhu, J., and Watkins, D., 1999. "The effects of joint clearance on position and orientation deviation of linkages and manipulators." *Mechanism and Machine Theory,* **35**(3), pp. 391–401.

[17] Wu, W., and Rao, S., 2004. "Interval approach for the modeling of tolerances and clearances in mechanism analysis." *J. Mech. Design,* **126**(4), pp. 581–592.

[18] Zhu, J., and Ting, K., 2000. "Uncertainty analysis of planar and spatial robots with joint clearances." *Mechanism and Machine Theory,* **35**(9), pp. 1239–1256.

[19] Choi, D., Lee, S., Wickert, J., and Yoo, H., 2006. "Statistical tolerance analysis of a robotic manipulator having uncertainties in joint clearance and axis orientation." *IEEE Transactions on Robotics*, Submitted.

[20] Lee, S., and Gilmore, B., 1991. "The determination of the probabilistic properties of velocities and accelerations in kinematic chains with uncertainty." *ASME J. Mech. Design,* **113**, pp. 84–90.

[21] Lee, S., Gilmore, B., and Ogot, M., 1993. "Dimensional tolerance allocation of stochastic dynamic mechanical systems through performance and sensitivity analysis." *ASME J. Mech. Design,* **115**, pp. 392–402.

[22] TRW, 1965. *Automotive Steering Linkages*., first ed. TRW, Warren, Michigan.

[23] Milliken, W., and Milliken, D., 1995. *Race Car Vehicle Dynamics*. SAE, Warrendale, PA.

[24] Leishman, R., and Chase, K. "Rack and pinion steering linkage synthesis using an adapted freudenstein approach." *ASME IDETC/CIE 2009* Accepted.

[25] Mitchell, W., Staniforth, A., and Scott, I., 2006. Analysis of Ackermann Steering Geometry Tech. Rep. 2006-01-3638, Motorsports Engineering Conference and Exposition, SAE, Dearborn, MI, December.

[26] Gillespie, T., 1992. *Fundamentals of Vehicle Dynamics*. SAE.

[27] Thompson, D., 2007. Ackerman? anti-ackerman? or parallel steering? On the WWW, August URL www.racing-car-technology.com.au/Steering%20Ackerman4.doc.

[28] Zapletal, E., 2001. "Running adrift." *Racecar Engineering,* **11**(7), pp. 37–47.

[29] Freudenstein, F., 1955. "Approximate sysnthesis of four-bar linkages." *Trans. ASME,* **77**(6), pp. 853–861.

[30] Chase, K., 1975. FREUDB: Interactive Linkage Design by Computer Refer to chasek@byu.edu for copy, August.

[31] Leishman, R., and Chase, K., 2009. A new tool for design and analysis of optimized rack and pinion steering mechanisms Tech. Rep. 2009-01-1675, Non-Conf. Spec. Tech. Papers, SAE, Warrendale, PA, June.

[32] Huo, H., and Chase, K., 1996. "Variation polygon - a new method for determining tolerance sensitivity in assemblies." In *Proc. CSME Forum*, CSME.

[33] Leishman, R., and Chase, K. "Variation analysis of position, velocity, and acceleration of two-dimensional mechanisms by the direct linearization method." *ASME IDETC/CIE 2009* Accepted.

[34] Glancey, C., 1994. "A Second-Order Method for Assembly Tolerance Analysis." MS Thesis, Brigham Young University, Provo, UT, December.

[35] Howell, L., 2001. *Compliant Mechanisms*. Wiley, New York, NY.

Appendix A

Screen Shots of the Steering System Design Tool

A.1 Steering Design and Analysis Tool Picutres

The following are some screen shot images of the steering design and analysis tool. The pictures help to understand the design and layout of the features on the tool, as mentioned in Chapter 3.

Figure A.1 shows the table where the vehicle input parameters are placed. As mentioned in Chapter 3, the inputs are hightlighted in blue, the outputs are in yellow, and the text of the solver parameter cells are in red.

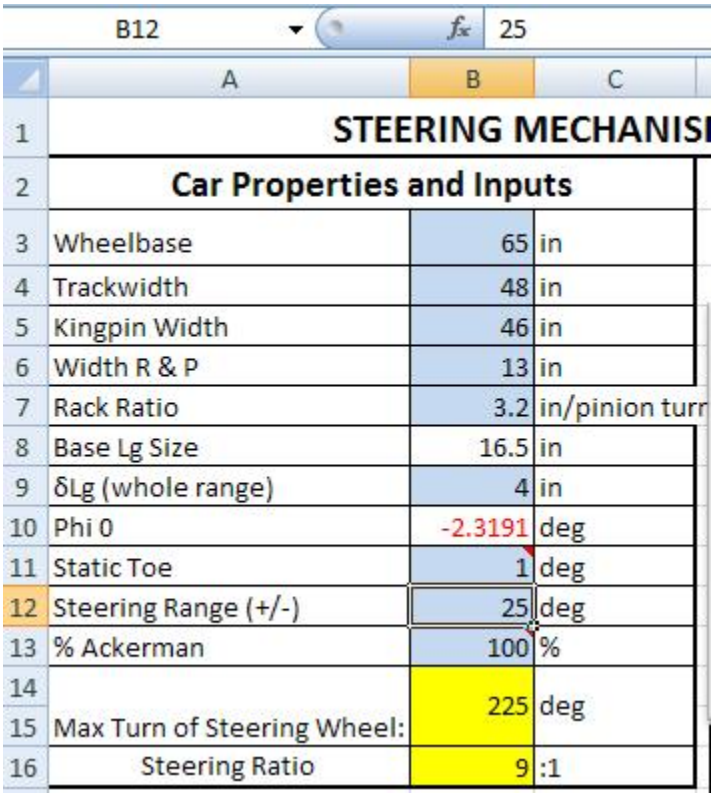

B12 | fx | 25

	A	B	C
1	STEERING MECHANISI		
2	**Car Properties and Inputs**		
3	Wheelbase	65	in
4	Trackwidth	48	in
5	Kingpin Width	46	in
6	Width R & P	13	in
7	Rack Ratio	3.2	in/pinion turr
8	Base Lg Size	16.5	in
9	δLg (whole range)	4	in
10	Phi 0	-2.3191	deg
11	Static Toe	1	deg
12	Steering Range (+/-)	25	deg
13	% Ackerman	100	%
14			
15	Max Turn of Steering Wheel:	225	deg
16	Steering Ratio	9	:1

Figure A.1: This table is where the input parameters are placed for the steering design tool.

Figure A.2 shows the table where the solver parameters are inserted. The constraint cells are shown at the top. The three possible target cells are shown in the middle of the figure: cells *Sum Sq. Errors (SSE) - Lead, SSE - Tol - Leading*, and *SSE - Trailing*. The precision points that are moved around by the solver, to synthesize the steering mechanism, are shown at the bottom of the figure.

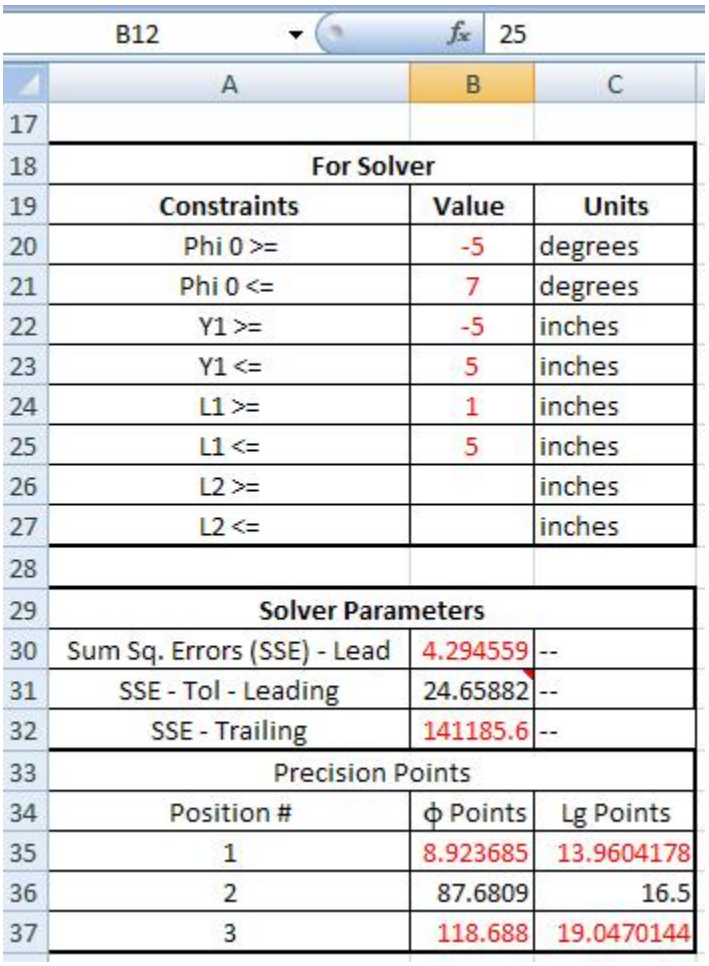

B12 | fx | 25

	A	B	C
17			
18	For Solver		
19	Constraints	Value	Units
20	Phi 0 >=	-5	degrees
21	Phi 0 <=	7	degrees
22	Y1 >=	-5	inches
23	Y1 <=	5	inches
24	L1 >=	1	inches
25	L1 <=	5	inches
26	L2 >=		inches
27	L2 <=		inches
28			
29	Solver Parameters		
30	Sum Sq. Errors (SSE) - Lead	4.294559	--
31	SSE - Tol - Leading	24.65882	--
32	SSE - Trailing	141185.6	--
33	Precision Points		
34	Position #	ϕ Points	Lg Points
35	1	8.923685	13.9604178
36	2	87.6809	16.5
37	3	118.688	19.0470144

Figure A.2: Solver parameters for the steering design tool.

The output link lengths and the cells where the tolerance and clearance values are input are shown in Fig. A.3.

All the other charts and graphs that are shown in the Steering Design Tool are shown in Chapters 2 and 3.

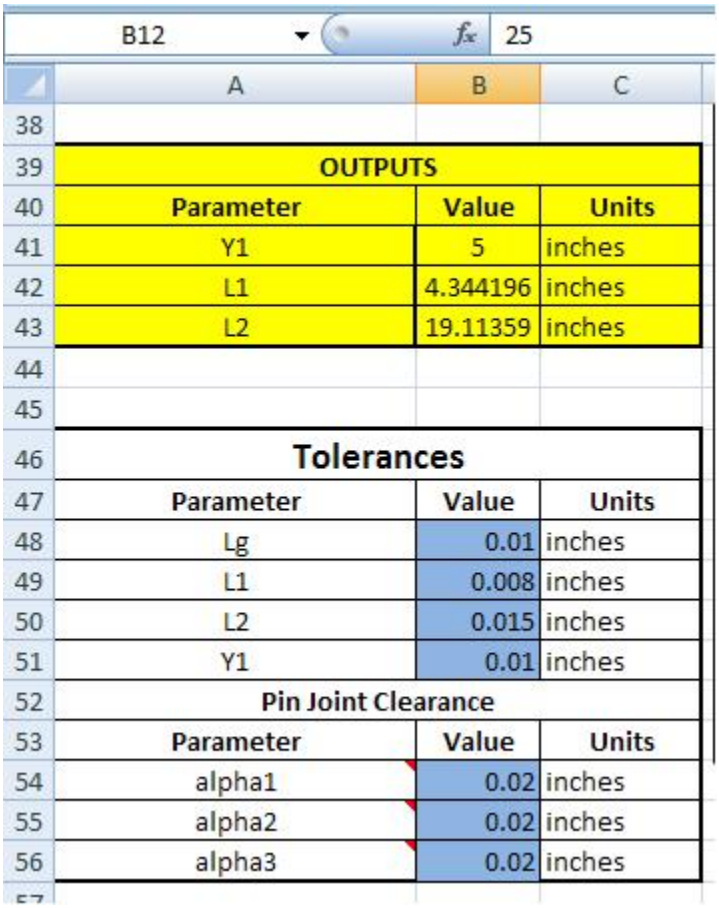

	A	B	C
38			
39	**OUTPUTS**		
40	**Parameter**	**Value**	**Units**
41	Y1	5	inches
42	L1	4.344196	inches
43	L2	19.11359	inches
44			
45			
46	**Tolerances**		
47	**Parameter**	**Value**	**Units**
48	Lg	0.01	inches
49	L1	0.008	inches
50	L2	0.015	inches
51	Y1	0.01	inches
52	**Pin Joint Clearance**		
53	**Parameter**	**Value**	**Units**
54	alpha1	0.02	inches
55	alpha2	0.02	inches
56	alpha3	0.02	inches

Figure A.3: Output link lengths for the steering design tool